



Glaciology – from field data to models

Dr. W.W. (Walter) Immerzeel

w.w.immerzeel@uu.nl

J. F. (Jakob) Steiner

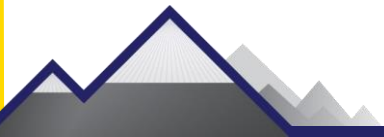
j.f.steiner@uu.nl

Hydrology, Climate Change and the Cryosphere



Topics

- Why do Glaciers matter?
- Theory
- Field Methods
- Remote Sensing of Glaciers
- Modelling - *Case Studies*





Literature

- Cuffey, K. M., & Paterson, W. S. B. (2010). *The physics of glaciers*. Burlington, MA, Butterworth-Heinemann/Elsevier.
- Greve, R., & Blatter, H. (2009). *Dynamics of Ice Sheets and Glaciers*. Springer
- Van der Veen, C.J. (2013). *Fundamentals of Glacier Dynamics*. Francis & Taylor
- Marshall, S.J. (2012). *The Cryosphere*, Princeton University Press
- Kargel, J. et al. (2013). *Global Land Ice Measurements from Space*. Springer



Topics

- Why do Glaciers matter?
- Theory
- Field Methods
- Remote Sensing of Glaciers
- Modelling - *Case Studies*



Glaciers Globally

Total Area:

RGI: 734 933 km²

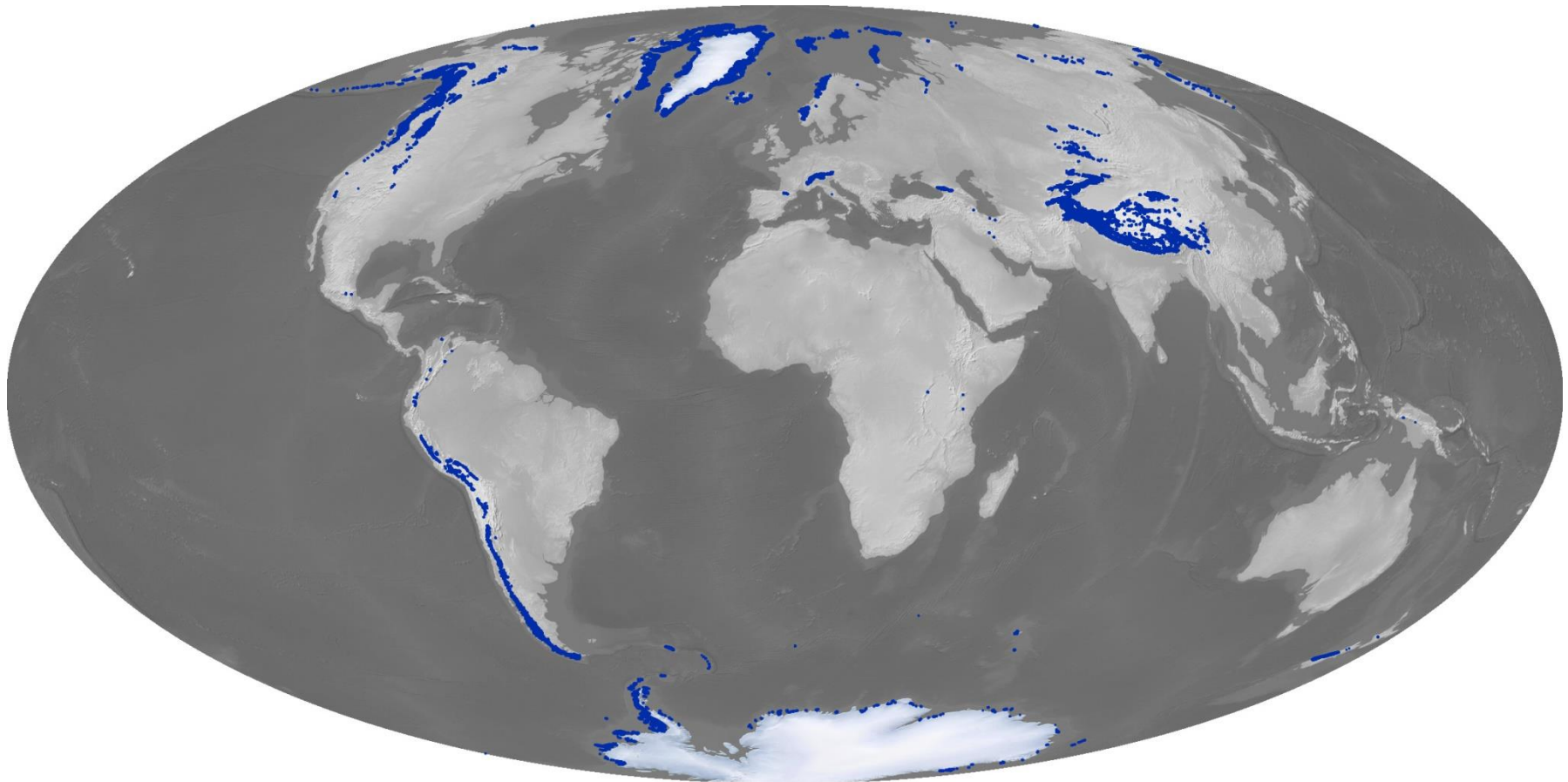
WGI: 747 688 km²

Volume (SLE, m):

Radic & Hock, 2010: 0.60 +/- 0.07

Huss & Farinotti, 2012: 0.43 +/- 0.06

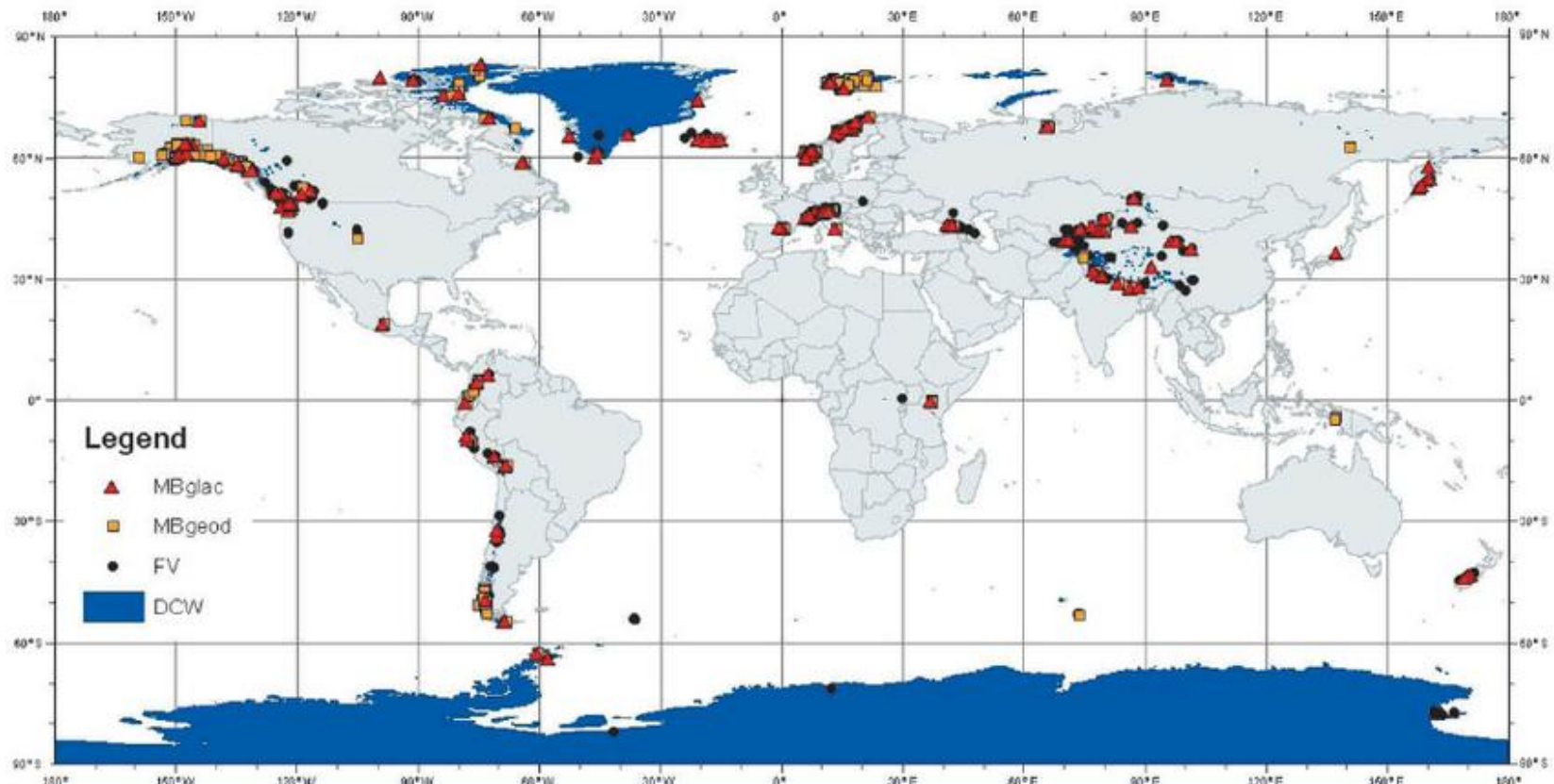
Grinsted, 2013: 0.35 +/- 0.07



R. Simmon, NASA; based on RGI4 (2013)



Measurements



Zemp et al., (2013) in *Global Land Ice Measurements from Space*, Springer



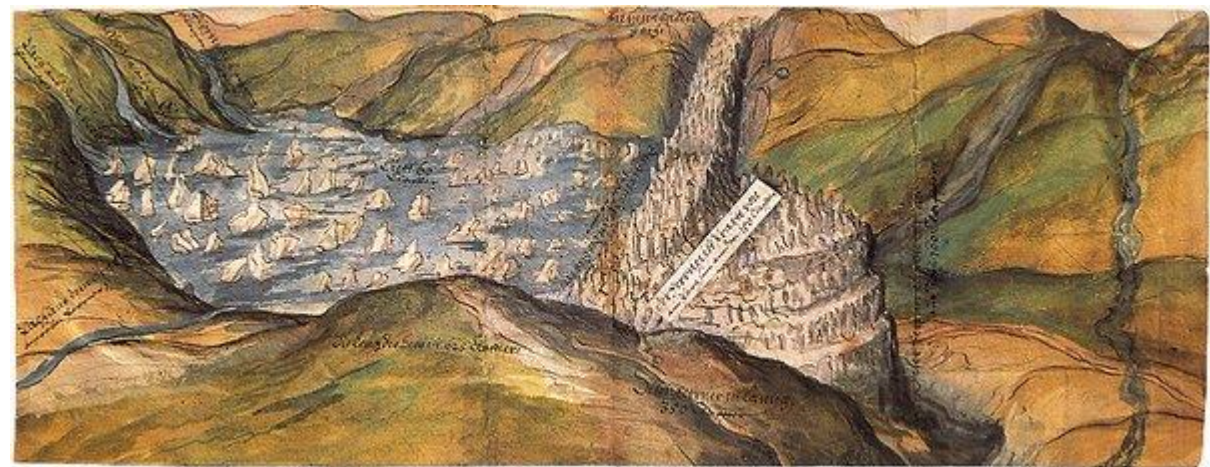
Why do we care? Resource and Risk

- Resource
 - Water Supply (Irrigation)
 - Hydropower
- Risk
 - Sea Level Rise
 - Glacial Lake Outburst Floods



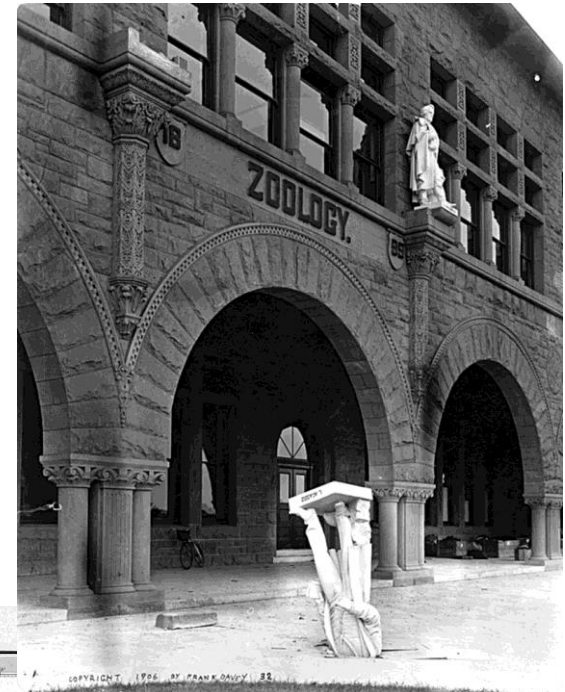
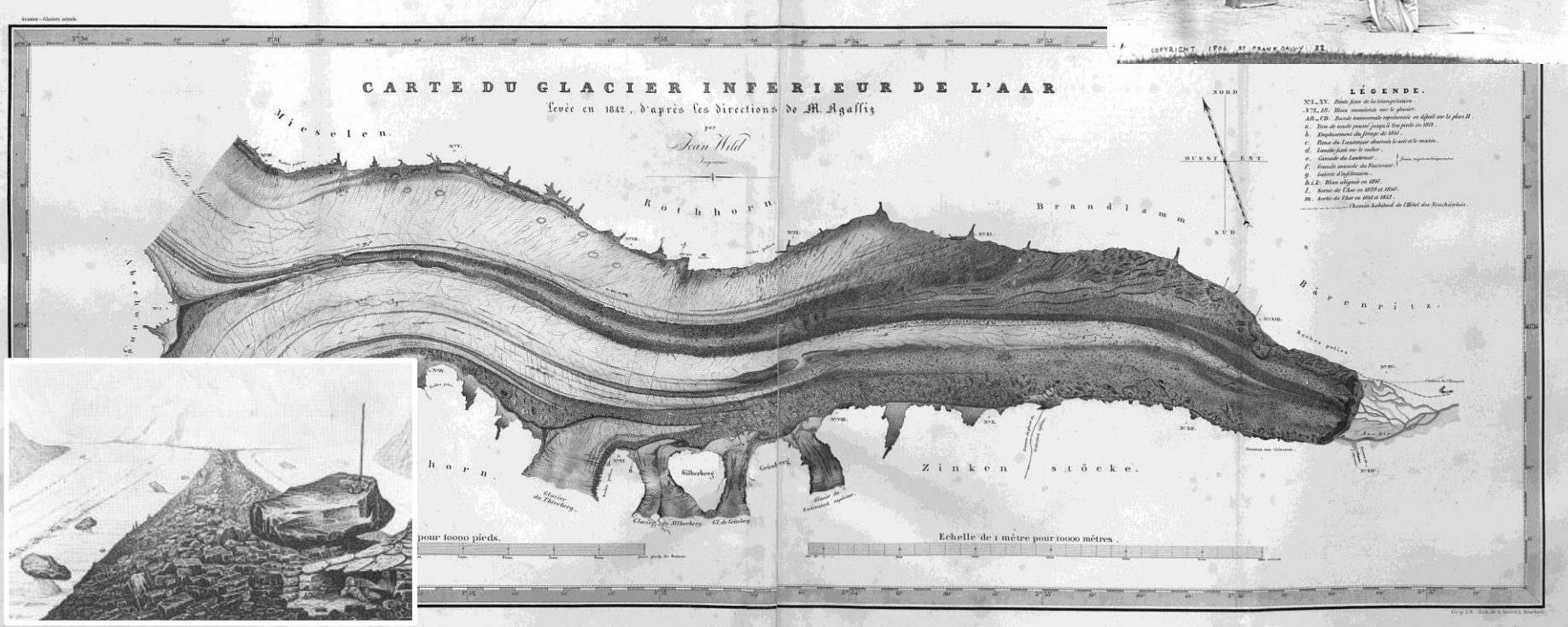
The first steps and failures

Vernagtferner, 1601



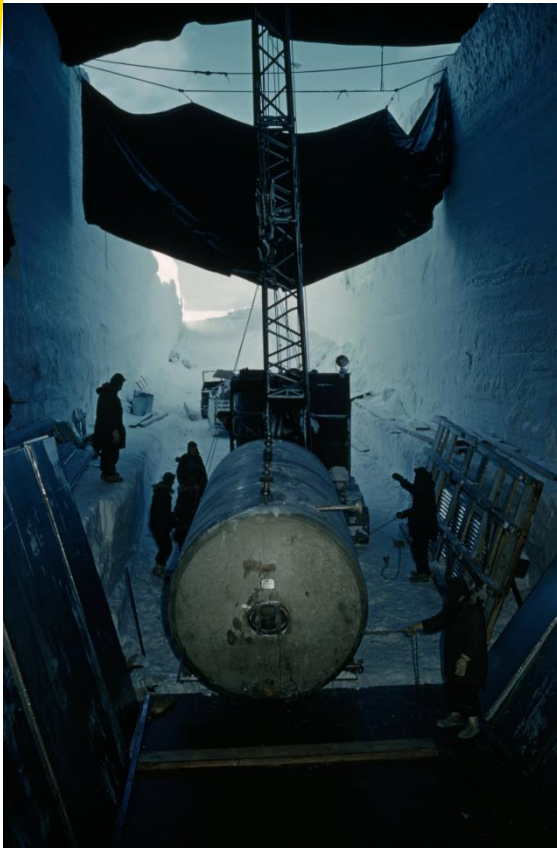


Louis Agassiz – Études sur les glaciers (1840)

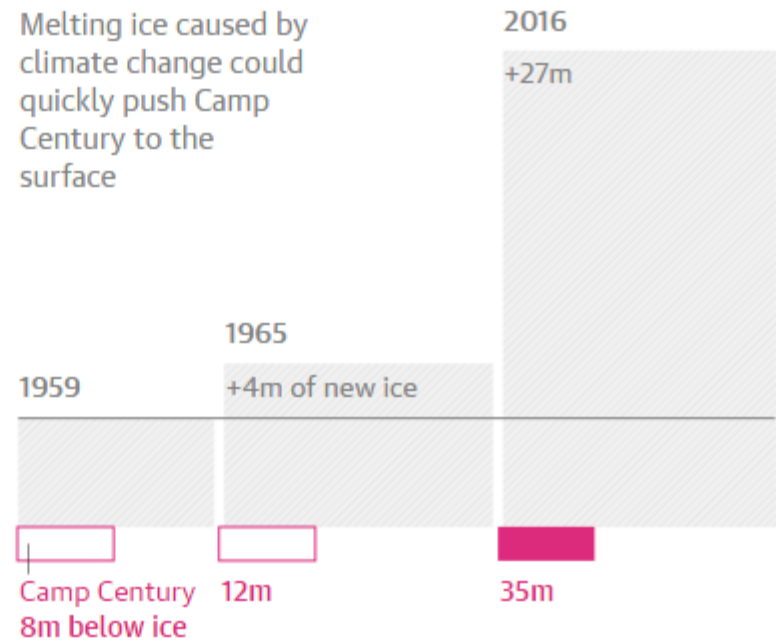




Camp Century – Project IceWorm



Melting ice caused by climate change could quickly push Camp Century to the surface



Graphic: The Guardian, 27/09/2016

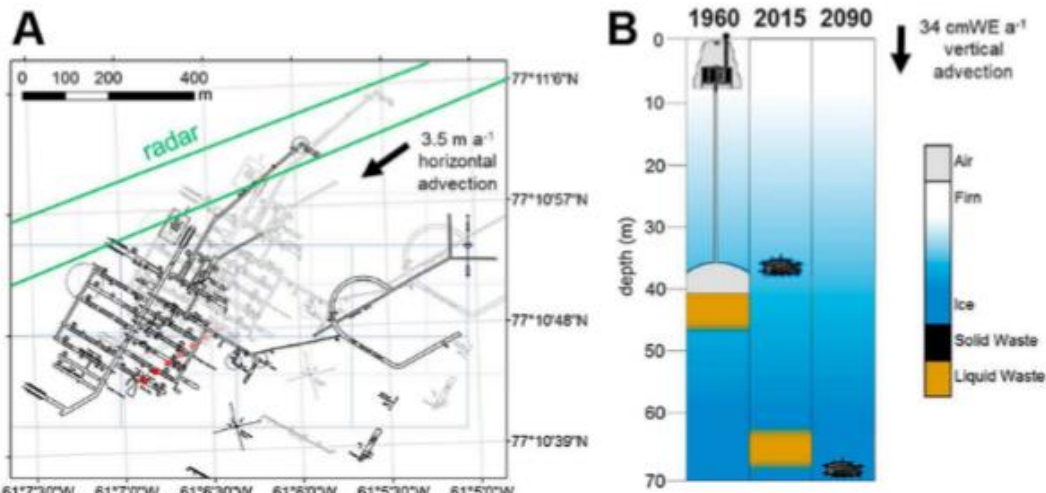


Figure 2. (a) Camp Century "as built" map georeferenced to 1960 (grey) and 2020 (black) locations [Kovacs, 1970], based on past surveys of the borehole location and horizontal advection associated with ice flow (Supplementary Methods). The red points denote decadal borehole location from 1960 to 2020. The green lines denote radar profiles shown in Figure 3. (b) Estimated Camp Century solid and refrozen liquid waste depths in 1960, 2015, and 2090, based on vertical advection rates (Figure S3). The horizontal extent of the liquid waste, while large relative to tunnel width, is small relative to camp width.



Colgan et al., 2016, GRL

Future Ice melt in a changing climate ...

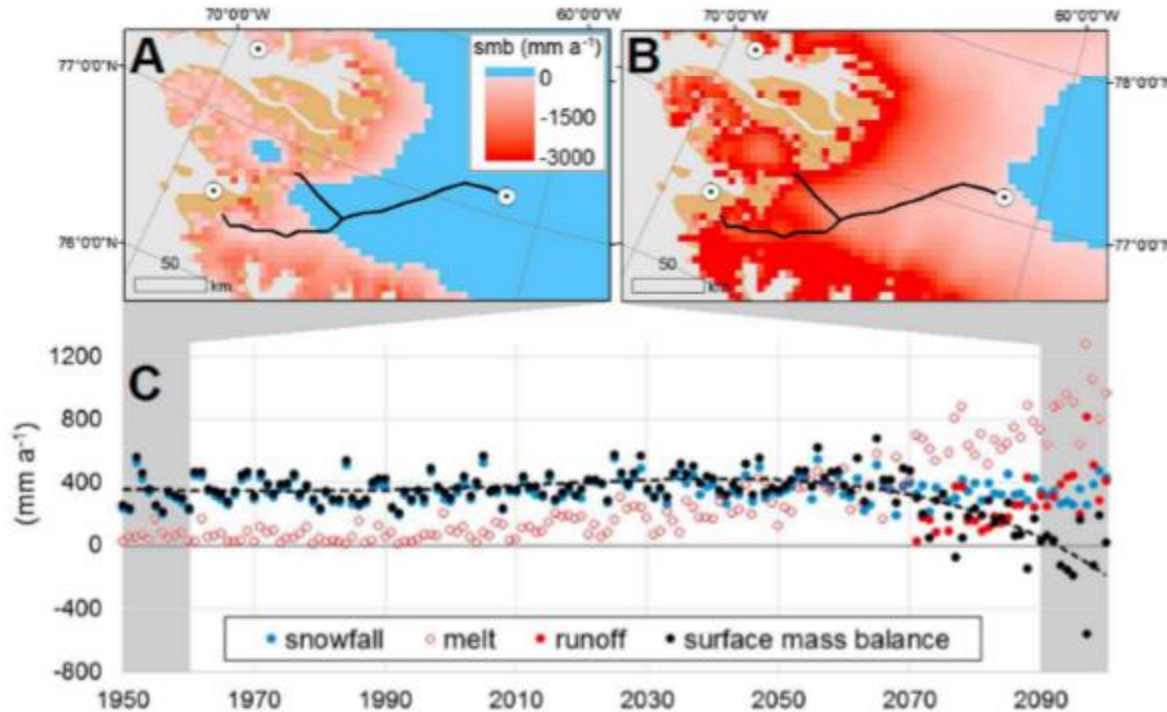


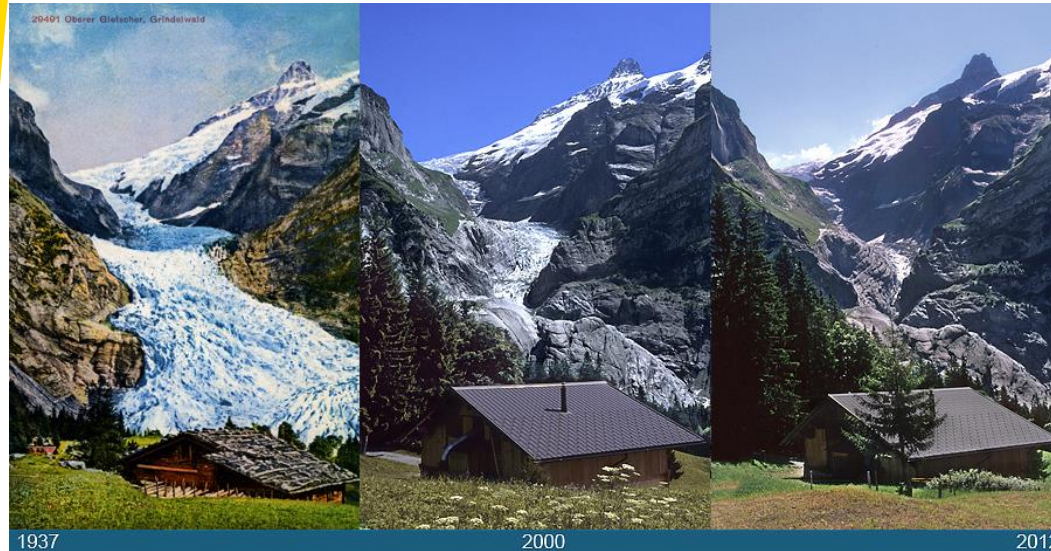
Figure 4. (a) Surface mass balance in Northwest Greenland during the 1950s (1950–1959) and (b) 2090s (2090–2099) as simulated by MAR v3.5 forced by CanESM2 under RCP8.5 [Fettweis et al., 2013]. The color bars saturate at minimum and maximum values. The blue shading denotes the accumulation area where surface mass balance is positive. (c) Surface mass balance, and its components, at Camp Century during 1950–2100 as simulated by MARv3.5 and forced by CanESM2. The dashed line denotes polynomial trend. The NorESM1 simulation is shown in Figure S2.

Colgan et al., 2016, GRL

... what about horizontal movement?



From Observations to Models



Year 2007 Rhone glacier



Grindelwaldgletscher (top) and Triftgletscher (bottom); Source: www.gletscherarchiv.de



Mass Balance Time Series

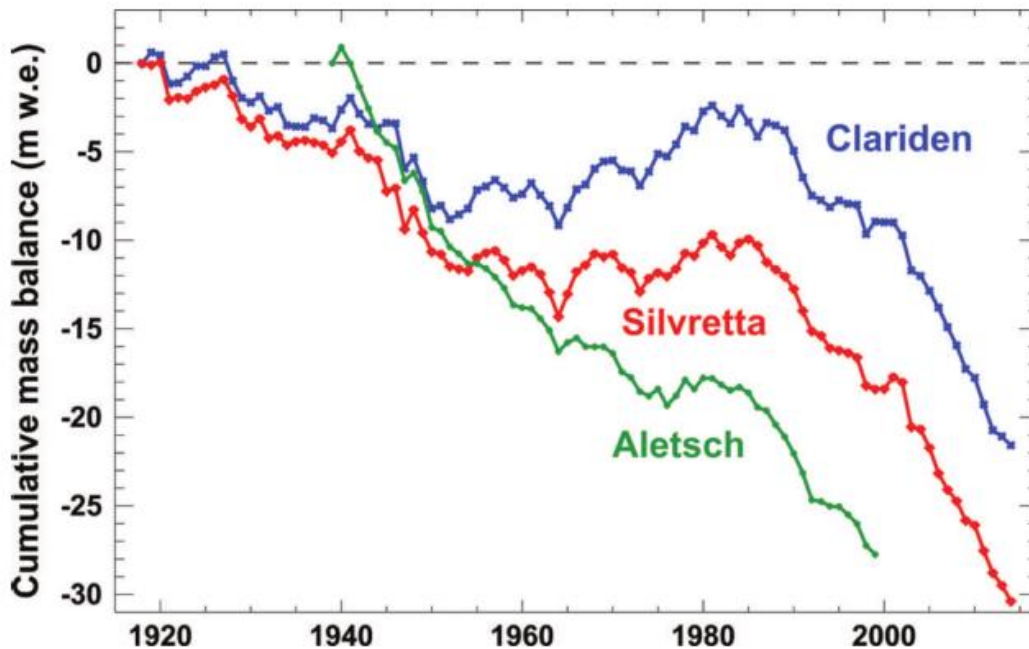


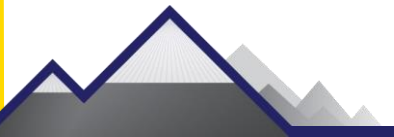
Fig. 4. Cumulative mass balance for Clariden and Silvretta (1918–2014) and Aletsch (1939–1999).

Huss et al., 2015 JoG



Topics

- Why do Glaciers matter?
- Theory
- Field Methods
- Remote Sensing of Glaciers
- Modelling - *Case Studies*





Elephant Foot Glacier,
NE - Greenland



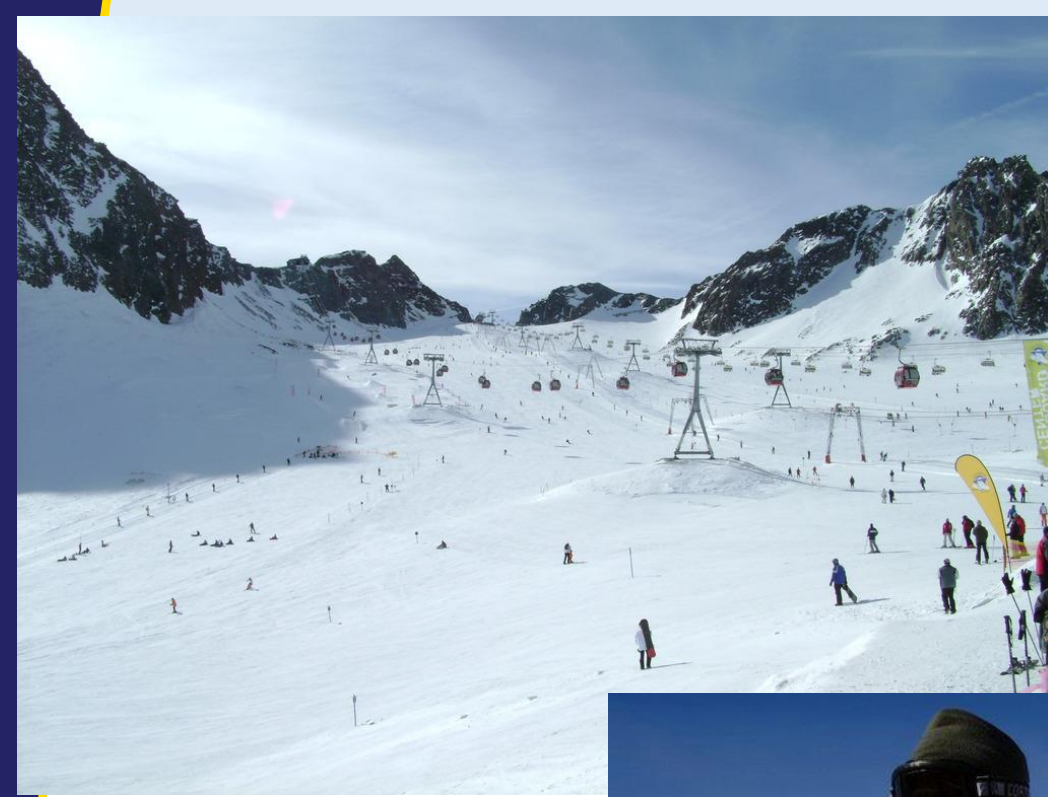
Baltoro Glacier,
Karakoram/Pakistan



Belvedere Glacier,
Val d'Aosta, Italian Alps



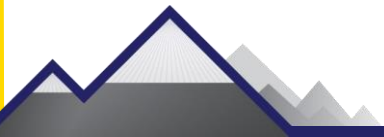
Furtwangler Glacier,
Kibo/Kilimanjaro,
Tanzania





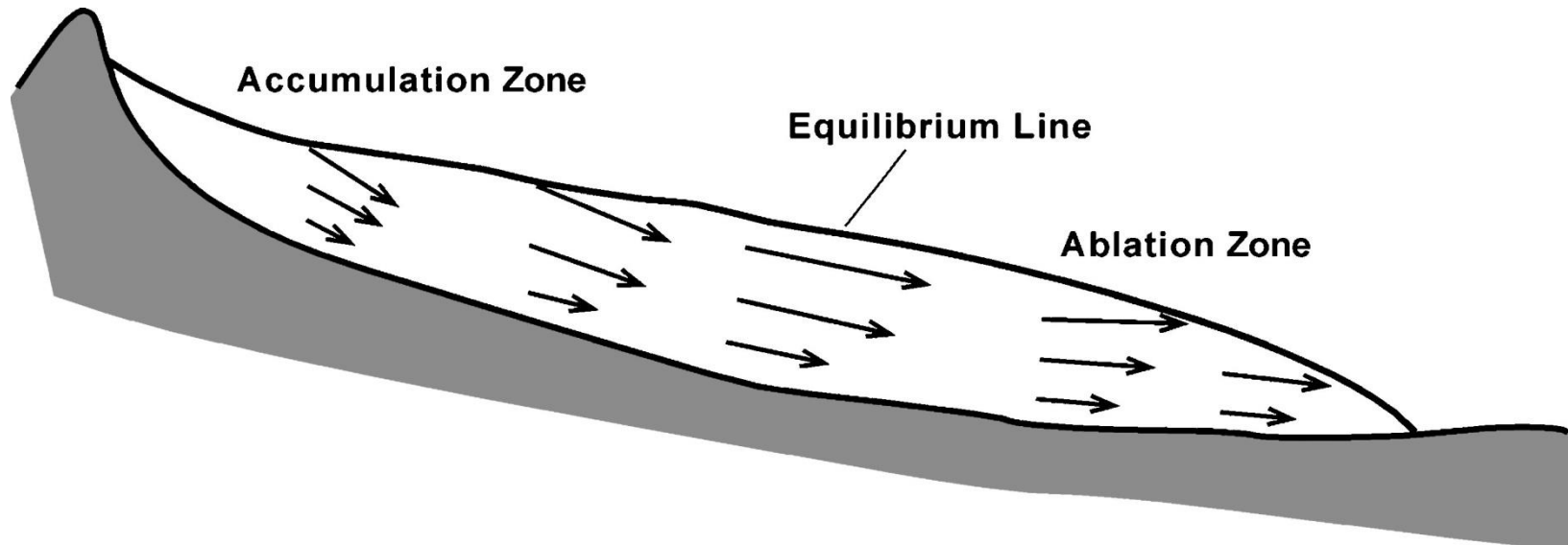
Theory

- Mass Balance
 - Principles
 - Field + Satellite Based Measurement Techniques
 - Mass Balance Gradient Model
- Energy Balance
 - Principles
 - Models for clean and debris covered glaciers
- Melt Models
 - Principles
 - Common examples
- Flow Dynamics





Mass Balance – Accumulation and Ablation



Cuffey and Patterson (2010)

- ELA – Equilibrium Line Altitude
- AAR – Accumulation Area Ratio ($= A_{Acc} / A_{total}$)

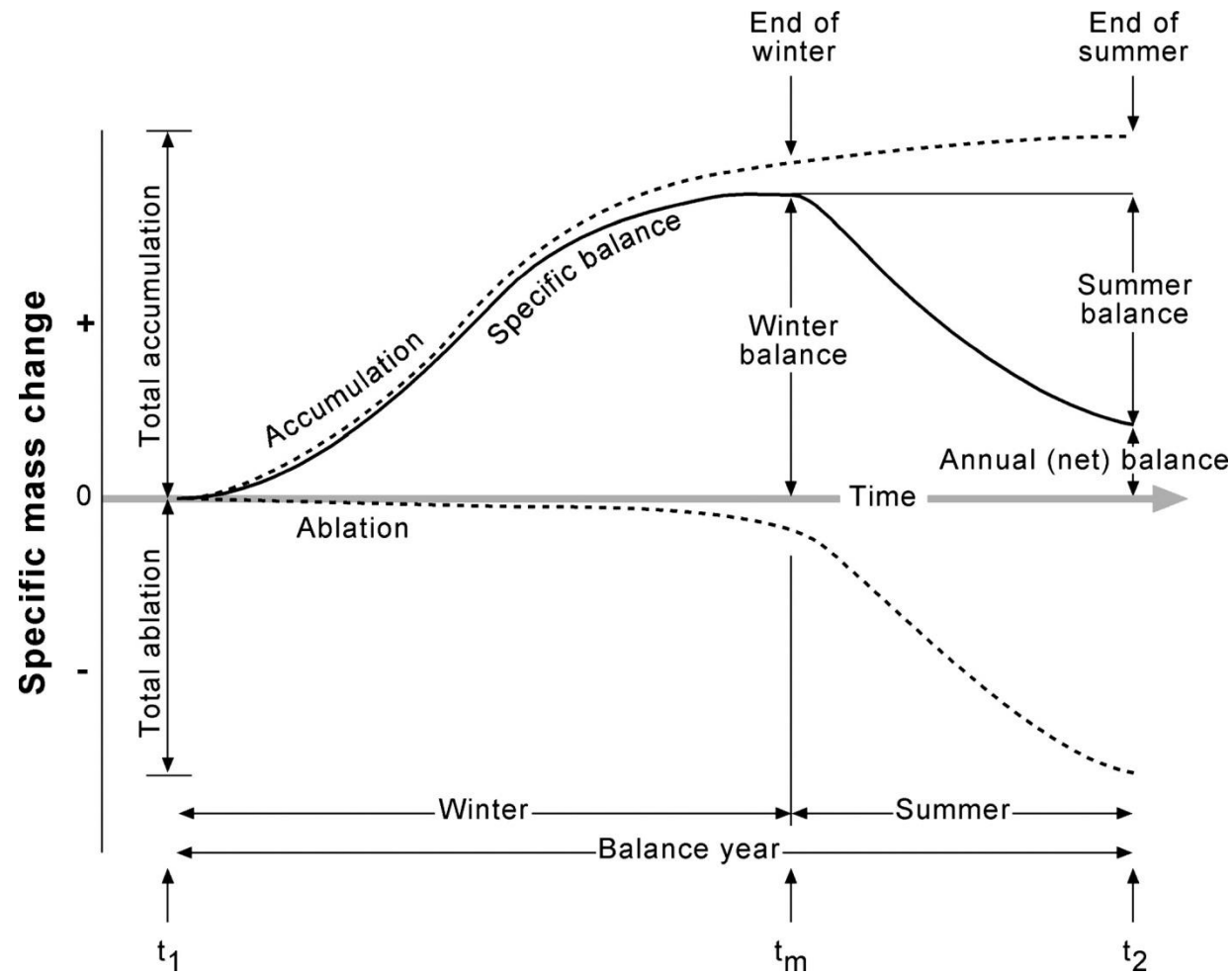


Mass Balance – Net Balance

Net Balance

$$b(\mathbf{x}) = \int_{t_1}^{t_2} \dot{b}(\mathbf{x}, t) dt \quad [\text{kg m}^2 \text{a}^{-1}]$$

$$B = \int_S b(\mathbf{x}) dS \quad [\text{kg}]$$



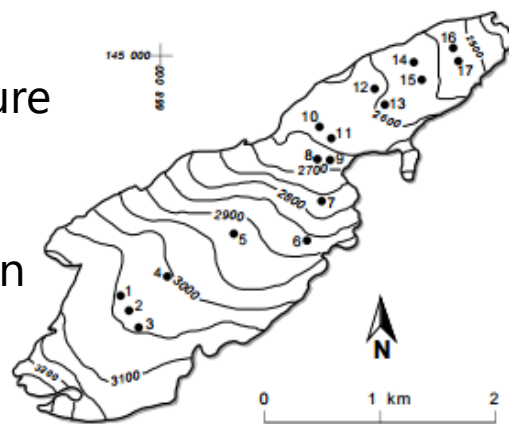
Cuffey and Patterson (2010)



Spatially Variable Mass Balance

Mountain Glaciers:

- Elevation Gradient of Precipitation/Temperature



Ice Sheets:

- Distance from the Ocean

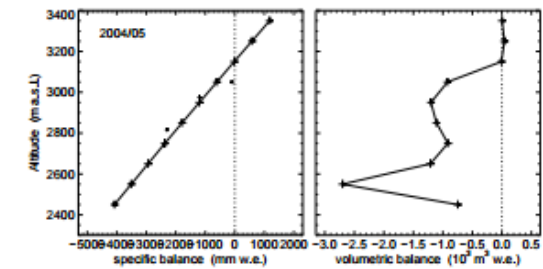
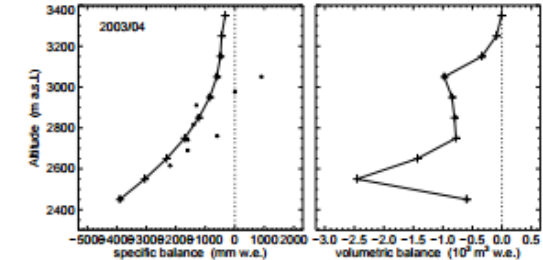
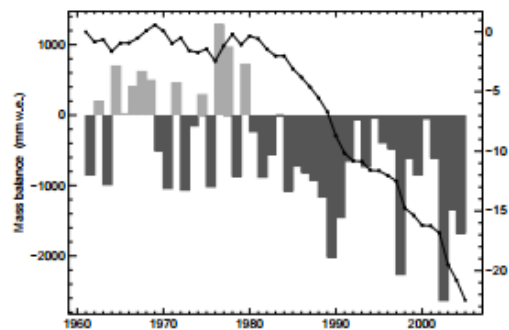


Figure 3.2: Mass balance data from Griesgletscher (Wallis, Switzerland). Top left: Map with mass balance stakes indicated, Bottom left: net mass balance 1961-2008, Right column: balance with respect to elevation (from Glaciological Reports, 2008).

Glaciological vs. Geodetic Mass Balance

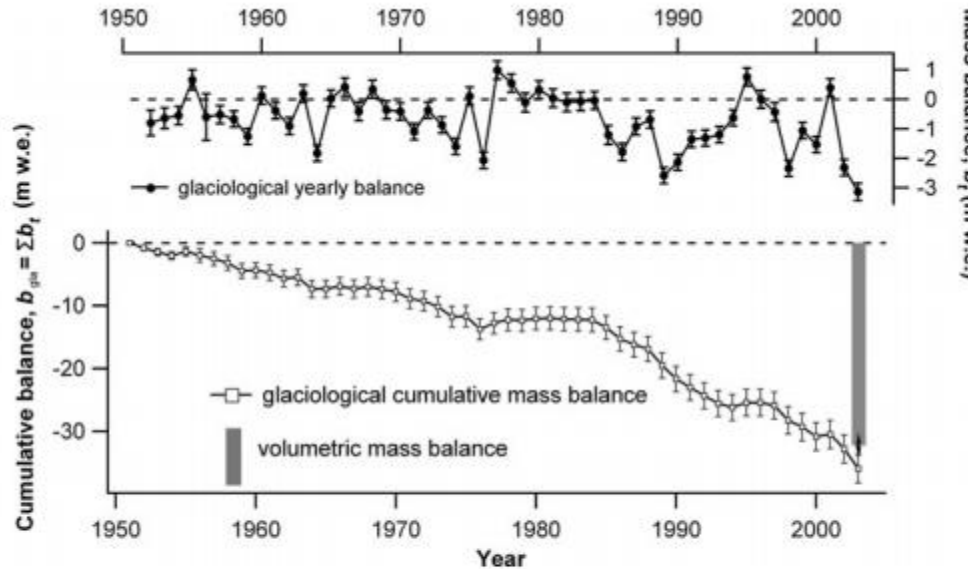


Fig. 3. Glaciological mass balances: upper curve is the glacier-wide yearly balances measured by the glaciological method and its annually calculated random errors according to the type of measurement. Lower curve is the cumulative glaciological mass balance and its comparison to the volumetric balance. No significant discrepancy between the two methods can be admitted at the $\alpha = 5\%$ type I error risk. Error bars are 1.96 standard deviations.

Thibert et al.. JoG, (2007)
Cogley, AoG, (2009)



Field Measurements

- Stake Readings (Accumulation, Ablation)
- Snow Pits (Density, Accumulation)



Claridenfirn, Switzerland
G. Kappenberger



Claridenfirn, Switzerland
G. Kappenberger





Geodetic Mass Balance

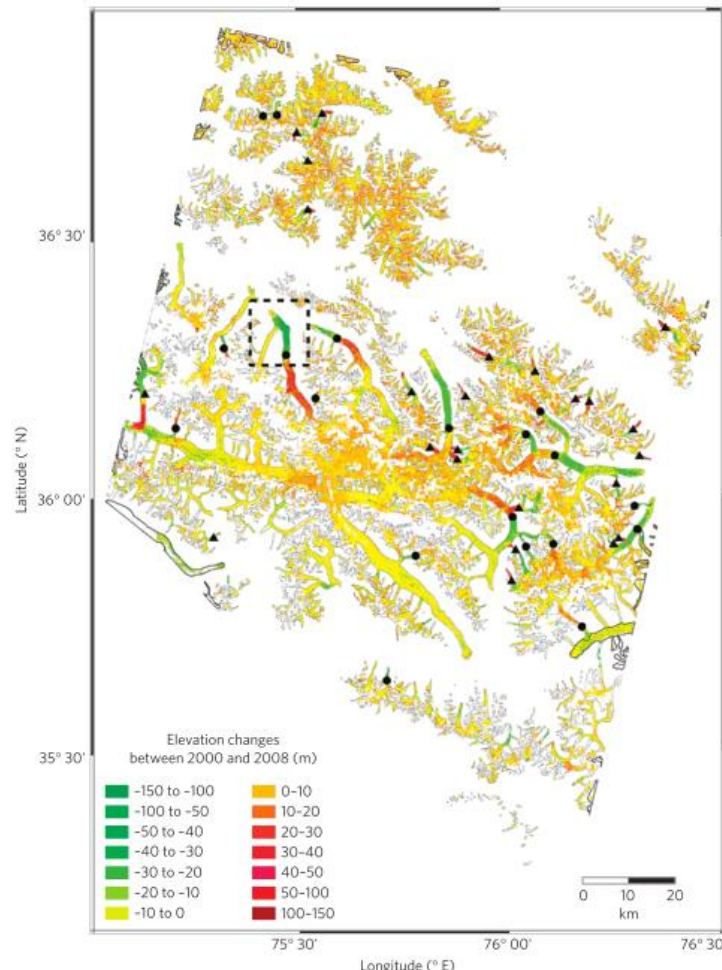


Figure 2 | Map of glacier elevation changes between February 2000 and December 2008. Grey polygons correspond to the glacier outlines (thick black polygons correspond to edge glaciers that were excluded from the mass-balance computation). The total ice-covered area is 5,615 km². The black triangles represent glaciers in a surge phase; black circles represent glaciers in a post-surge or quiescent phase. The dashed black box defines the area shown in Supplementary Fig. S1. 41% of elevation changes do not exceed ±5 m. Elevation differences off-glaciers are shown in Supplementary Fig. S4.

Gardelle et al., NatGeo (2012)



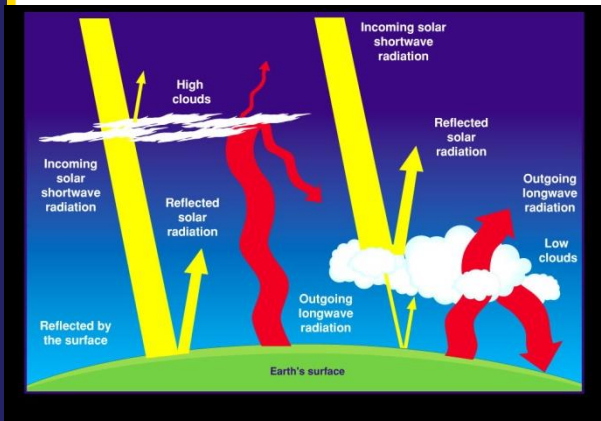
Energy Balance

- ... to melt ice we need Energy

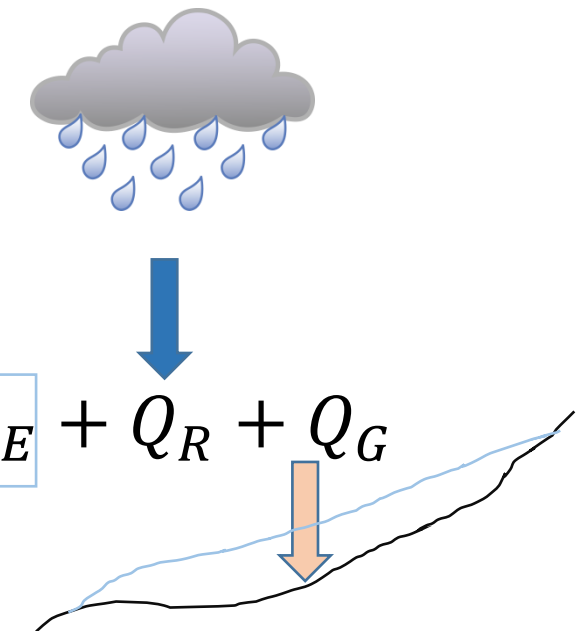
$$h_{we} \text{ [m w.e.]} = \frac{E \text{ [J]}}{\rho_w \text{ [kg m}^{-3}\text{]} L_f \text{ [J kg}^{-1}\text{]}}$$

$$Q_M \text{ [W m}^{-2}\text{]} = \frac{\delta E \text{ [J]}}{\delta t \text{ [s]}}$$

$$Q_M = \boxed{Q_{SW} + Q_{LW}} + \boxed{Q_H + Q_{LE}} + Q_R + Q_G$$



Radiative fluxes



Turbulent fluxes



Shortwave Radiation

$$Q_M = Q_{SW} + Q_{LW} + Q_H + Q_L$$

$$Q_{SW} = Q_I [W\ m^{-2}] (1 - \alpha [-])$$

the Solar Constant – 1376 W m⁻²

- Atmospheric Refraction
- Clouds

Albedo

- Black body = 0 / White Body = 1
- Snow: 0.2 – 0.9
- Ice: 0.1 – 0.5
- Debris: ?

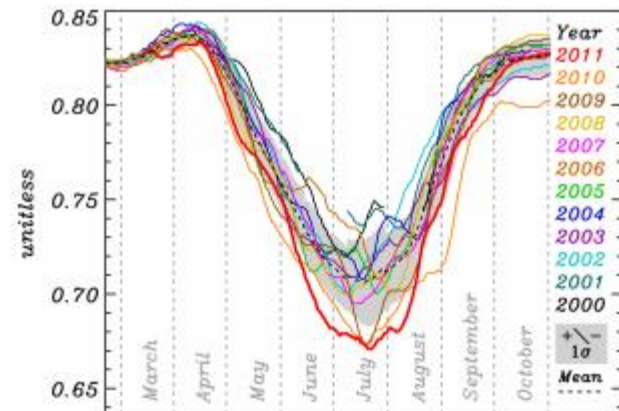


Fig. 6. 11-day running median Greenland ice sheet albedo from Moderate Resolution Imaging Spectroradiometer (MODIS) MOD10A1 data

Box et al., TC (2012)





Longwave Radiation

$$Q_M = Q_{SW} + Q_{LW} + Q_H + Q_L$$

$$Q_{LW} = LW_{in} - LW_{out}$$

$$LW_{in/out} = \varepsilon [-] \sigma [W m^{-2} K^{-4}] T^4_{air/surf} [K^4]$$

- Emissivity (ε): 0.85 – 1
- Stefan Boltzmann Constant (σ): $5.6703 * 10^{-8}$
- Sources of incoming LW:
 - Clouds
 - Mountain Slopes
 - Surrounding Debris



Sensors



Net Radiometer (SW)



Albedometer (SW)



CNR1 (SW + LW)



Turbulent Fluxes

Sensible Heat – Flux of Heat Energy by conduction and convection

$$Q_H = \rho [kg\ m^{-3}] c_p [J\ kg^{-1}K^{-1}] C_H u [m\ s^{-1}] (T_a - T_s) [K]$$

Latent Heat – Flux of Heat Energy with evaporation and condensation

$$Q_{LE} = \rho [kg\ m^{-3}] L [J\ kg^{-1}] C_L u [m\ s^{-1}] (e_a - e_s) [kPa]$$

- C_H and C_L are exchange coefficients that incorporate stability criteria of the SBL
 - includes surface roughness (z_0)
- c_p – specific heat of air
- L – latent heat of evaporation



Sensors





Which direction do the fluxes go?

$$Q_M = Q_{SW} + Q_{LW} + Q_H + Q_{LE} + Q_R + Q_G$$



The complication of Debris Cover

- Energy Transfer through the debris ...





Heat Conduction through debris

- Interaction of debris with atmosphere
- Wetting and drying of soil

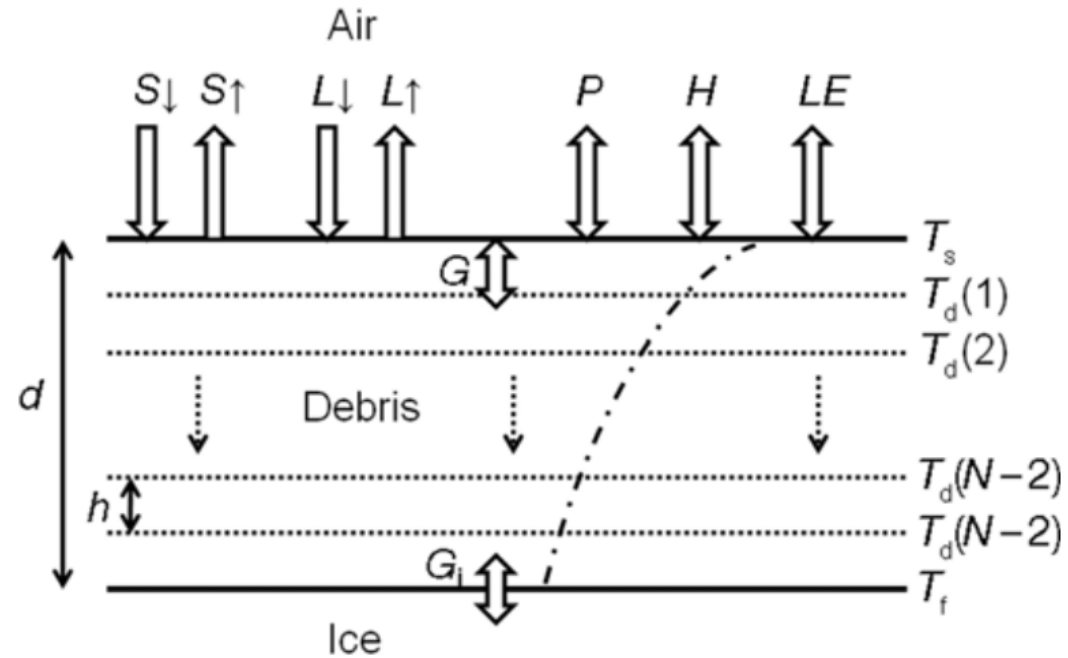


Fig. 1. Schematic of the DEB model showing heat fluxes at the top and bottom of a debris layer of thickness d . The debris temperature is calculated for N layers of thickness h , with boundary conditions defined by the surface temperature, T_s , and the temperature of the debris/ice interface, which is assumed to stay at $T_f = 0^\circ\text{C}$. The dash-dot curve is an example temperature profile, where temperature increases towards the right. Reid and Brock, JoG (2010)

- Debris Cover heats up
- Spatially variable
- What about thickness?

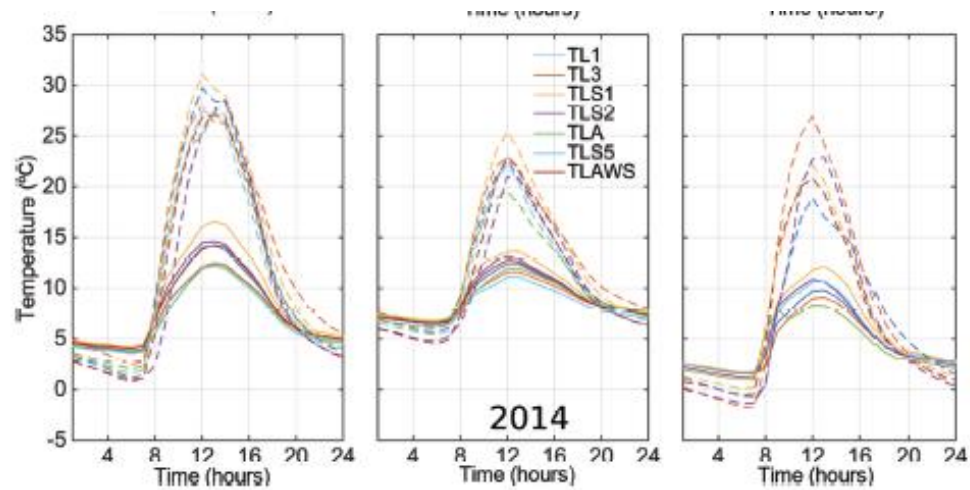


Fig. 9. Diurnal cycles of all T-Loggers in 2012, 2013 and 2014. Solid lines indicate air temperature while dashed lines indicate surface temperature. (a) Pre-monsoon season; (b) monsoon season; and (c) post-monsoon season.

Enhanced Melt on Cliffs and Ponds



Fig. 3. Photographs of cliffs 1 and 2 in May (top) and October (bottom) with the respective stake locations, each time taken from a similar position. Notice that, on cliff 1, stake 1.3 in May is at the same location as stake 1.1 in October. On cliff 2, stakes 2.1–2.3 are at approximately the same locations in both seasons.



Simpler Melt Models

- Classical Temperature Index

DDF [$\text{mm } d^{-1} \text{ } C^{-1}$]

$$M = \begin{cases} \frac{1}{n} \text{DDF}_{\text{ice/snow}} T_a & : T_a > T_T \\ 0 & : T_a \leq T_T \end{cases}$$

Gabbi et al., JoG (2014)
Hock, JoG (1999)
Pellicciotti et al., JoG (2005)

- HTI

RTI [$\text{mm m}^2 \text{ h}^{-1} \text{ W}^{-1} \text{ C}^{-1}$]

$$M = \begin{cases} (\text{MF} + R_{\text{ice/snow}} I_{\text{pot}}) T_a & : T_a > T_T \\ 0 & : T_a \leq T_T \end{cases}$$

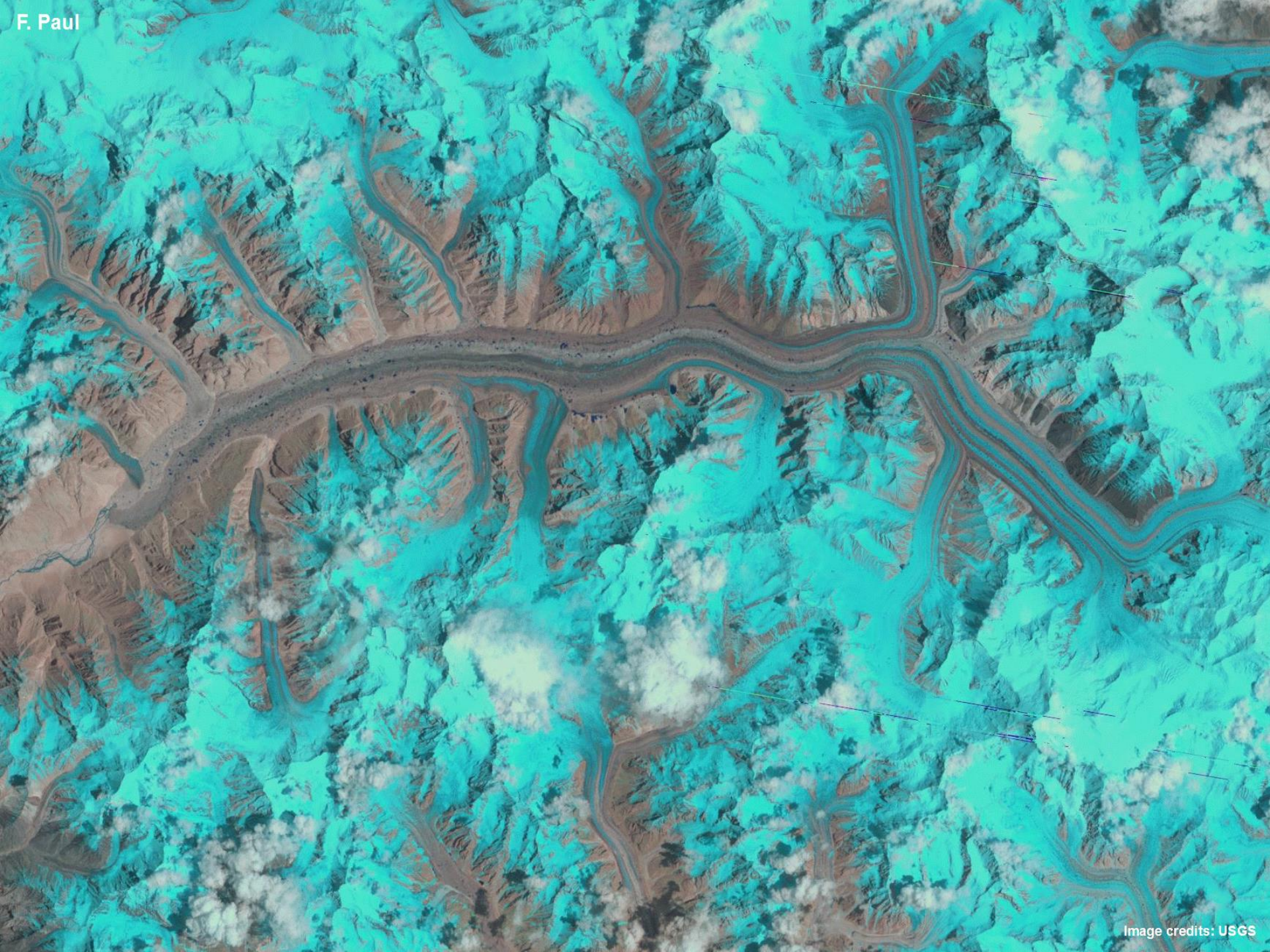
- ETI

TF [$\text{mm h}^{-1} \text{ C}^{-1}$]

$$M = \begin{cases} \text{TF} T_a + \text{SRF}(1 - \alpha) I & : T_a > T_T \\ 0 & : T_a \leq T_T \end{cases}$$

SRF [$\text{mm m}^2 \text{ h}^{-1} \text{ W}^{-1}$]

F. Paul



F. Paul

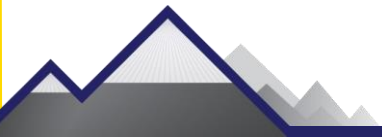


Image credits: USGS



Physics of Glacier Movement

- Plastic deformation – water pressure
- Basal Slip – basal temperatures
 - Basal velocity
 - Shear Stress
 - Water Pressure and Volume at Bed
 - Bedrock Topography
 - Sediment Properties
- But we only see surface velocity and past evidence on bed rock





$$\tau_b = \psi u_b$$

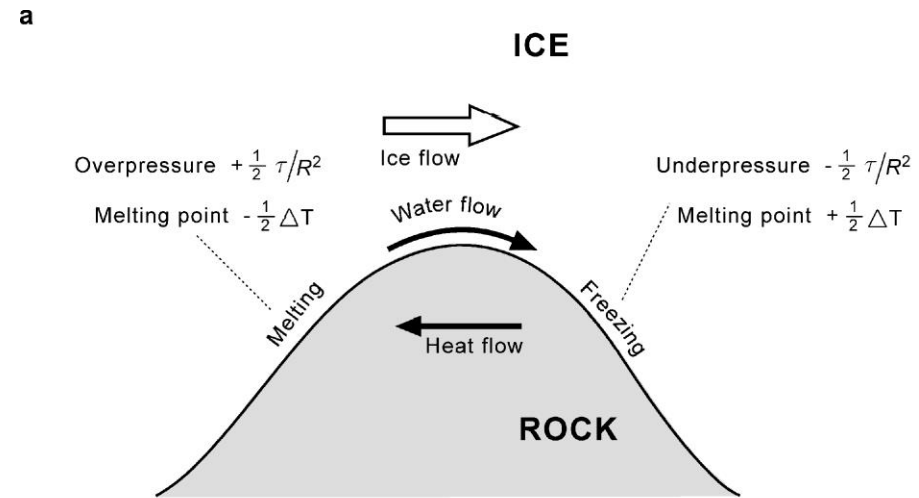
basal shear stress rate of slip



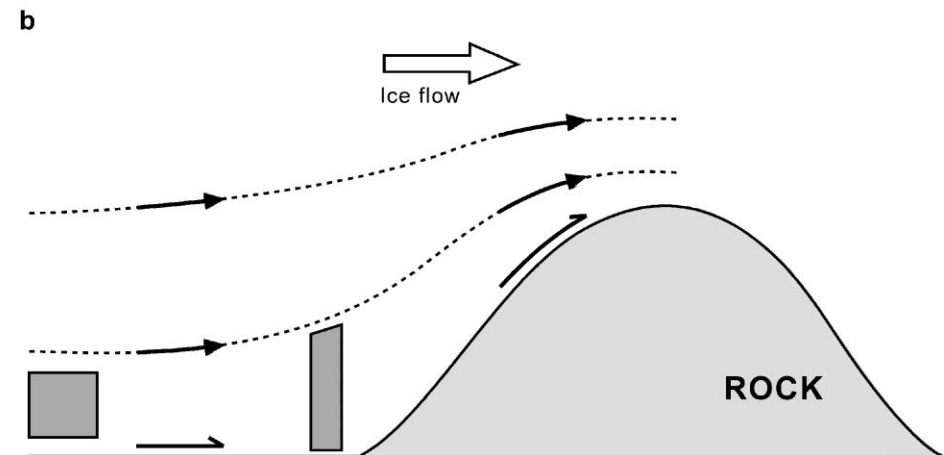


Weertman Sliding

- Regelation



- Enhanced Creep




$$\dot{\epsilon} = A\tau^n$$

$\dot{\epsilon}$... shear strain rate

τ ... shear stress

$$A = f(T)$$

- Glen's Law

- ... ice is not just "cold"
- Ice softens when it warms

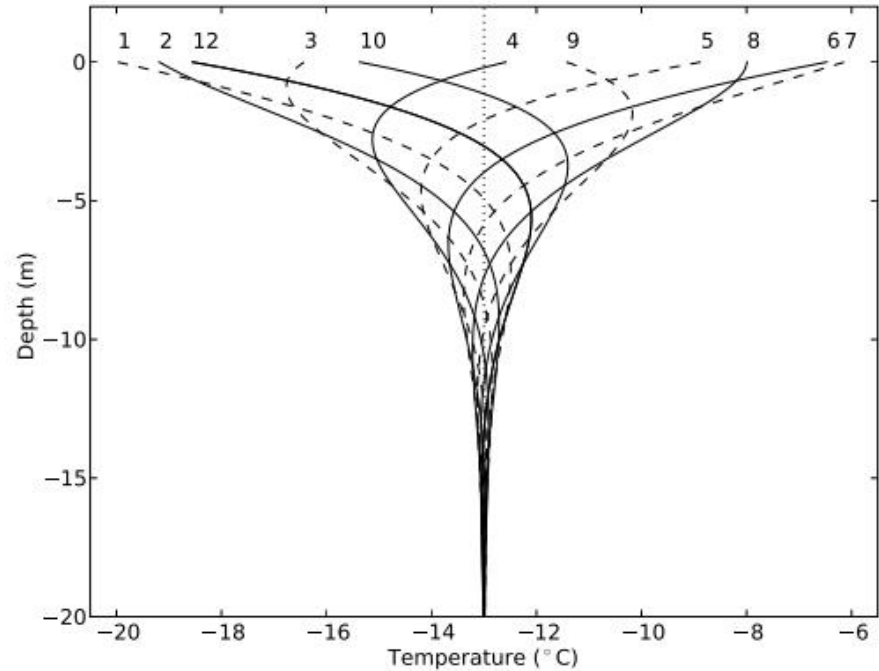
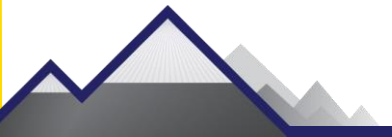


Figure 6.1: Variation of temperature with depth for the conditions at Colle Gnifetti. Numbers next to curves indicate months (1 corresponds to January).



Topics

- Why do Glaciers matter?
- Theory
- Field Methods
- Remote Sensing of Glaciers
- Modelling
- *Case Studies*





Field Methods

- AWS
- Melt / Mass Balance Measurements
- Ice Cores + Velocity/Temperature Profiles + GPR
- Subglacial Hydrology (Tracers)
- UAV (DEM, Velocity Fields – SfM)

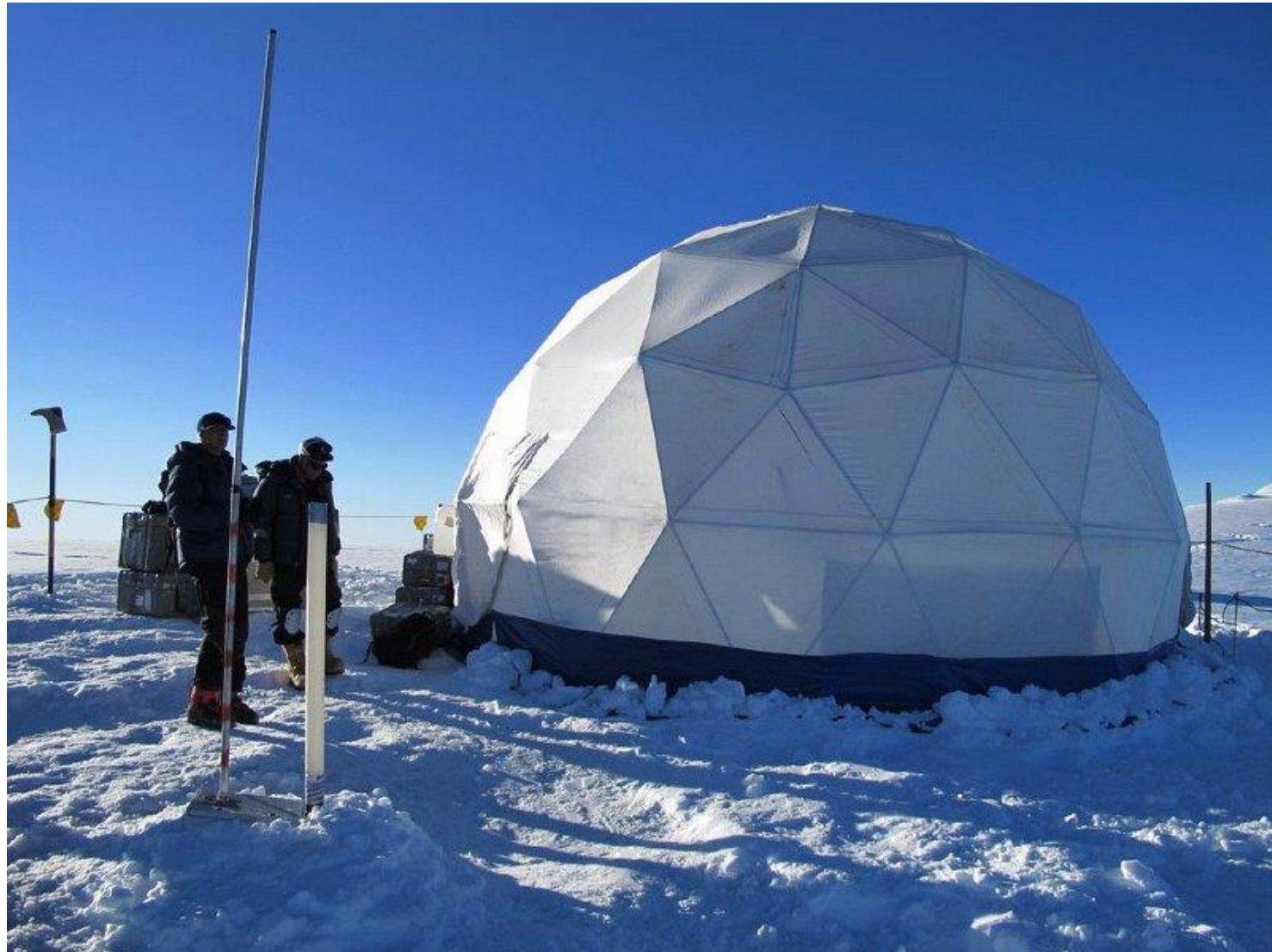


Sensors on Glaciers

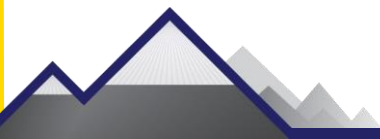




Inside the Glacier ...



Ortles Project
European Alps



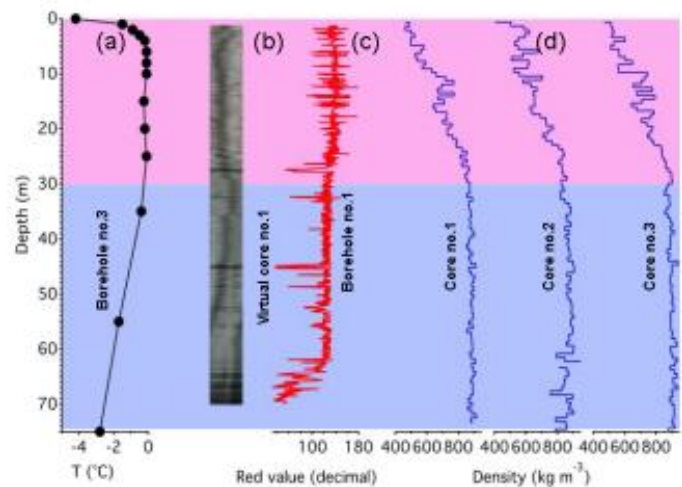


Figure 7. Physical characteristics of the Mt. Ortles cores. The temperate firn portion is enclosed in red shading, while the cold ice is in blue. (a) Borehole no. 3 temperatures recorded 43 days after the end of the drilling operations (from Gabrielli et al., 2012). (b) Virtual image of core no. 1 reconstructed from 360° Televiwer visual scanning of borehole no. 1. (c) Red component of the RGB digital signal obtained by means of visual scanning. High values indicate higher light reflection. (d) Densities of the Mt. Ortles ice cores no. 1, no. 2 and no. 3.





Glacier Thickness

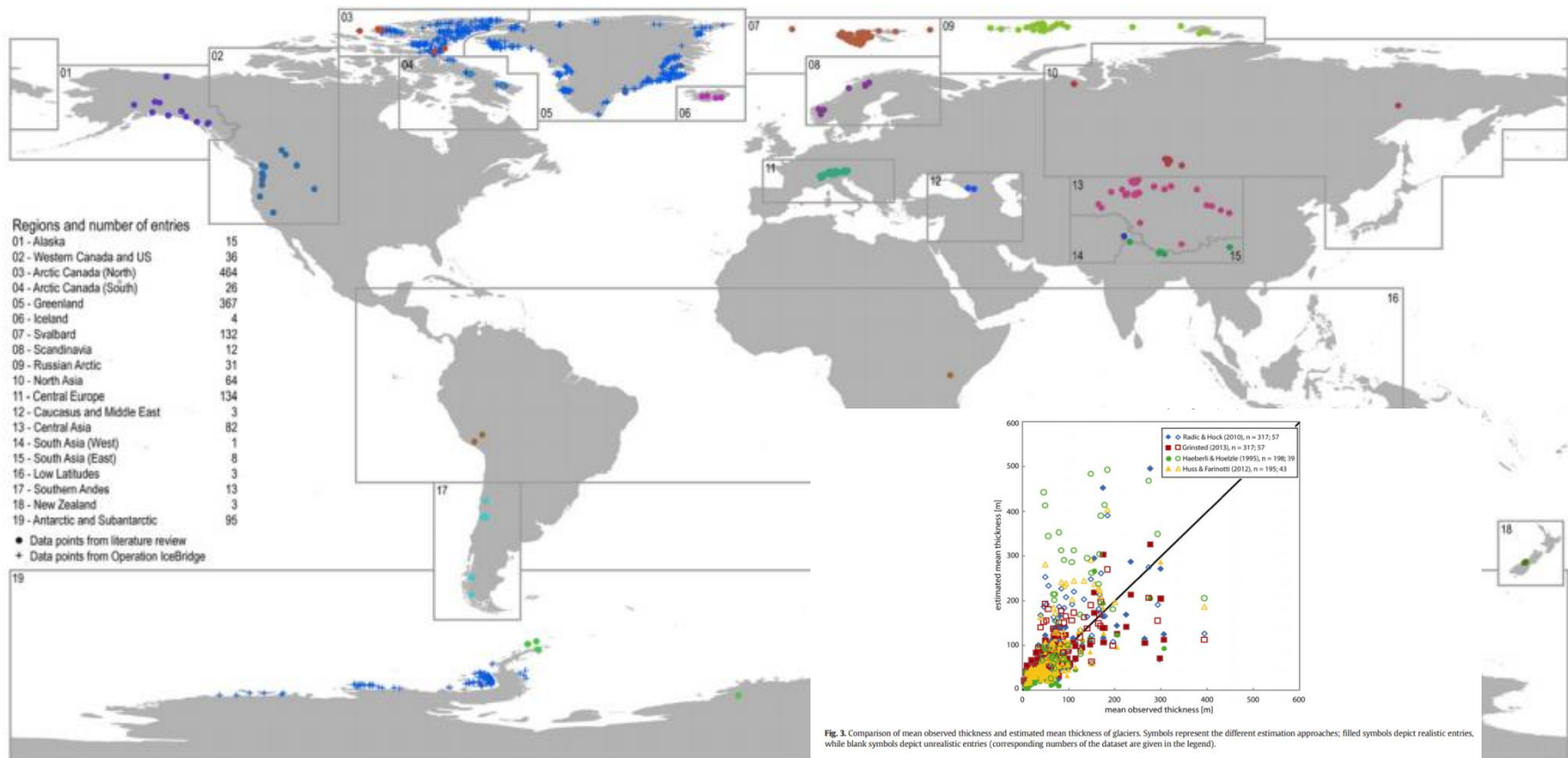


Fig. 2. Global and regional distribution of all compiled thickness observations. The crosses represent data from the Operation IceBridge. The dots represent data from literature review; the different colors underline the 19 different regions as based on Pfeffer et al. (2014).

GPR Measurements

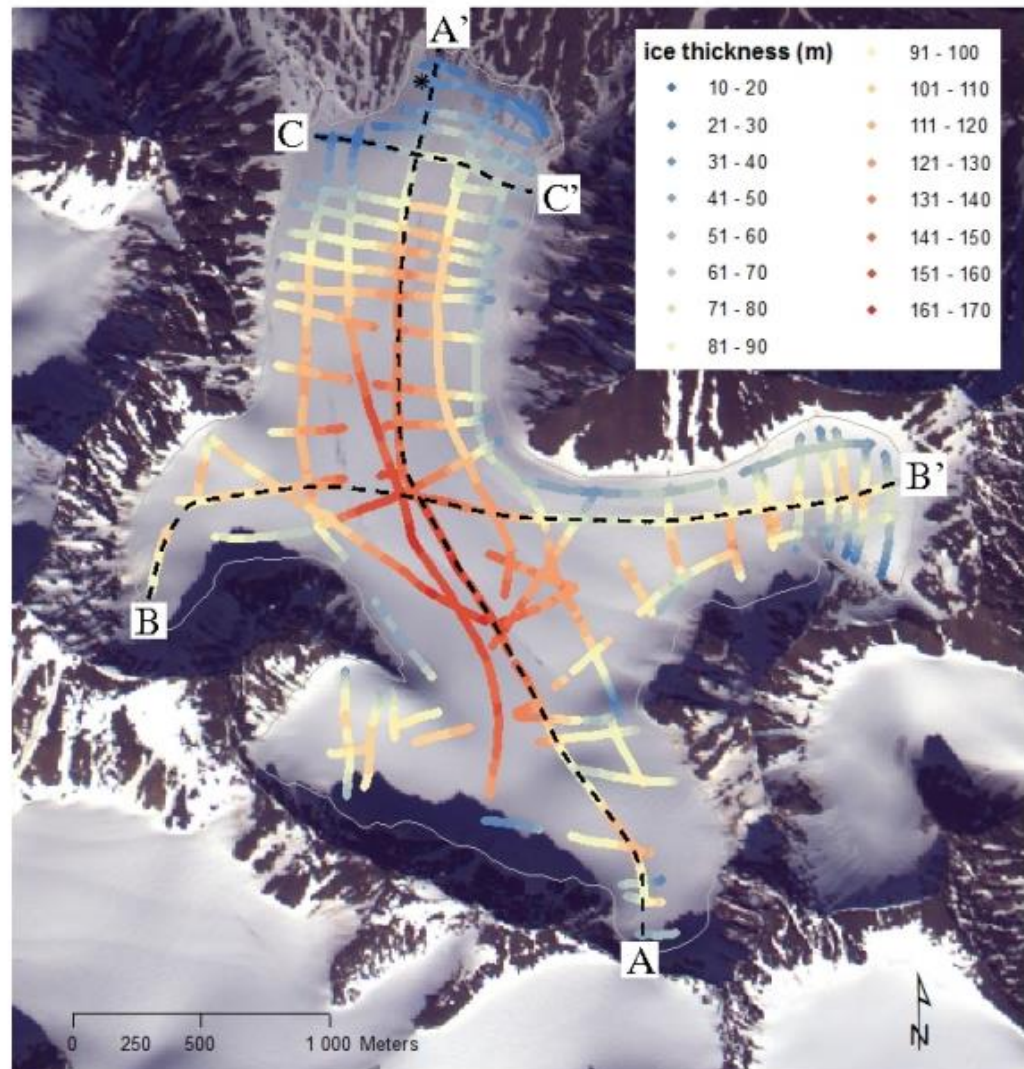


Fig. 1. GPR profiles over the Austre Lovénbreen (background image copyright FORMOSAT). The color scale indicates the ice thickness measured on each profiles. Dashed lines indicate GPR transects displayed on Fig. 4 to 7. The symbol * indicates the CMP position.



GPR - Radargram

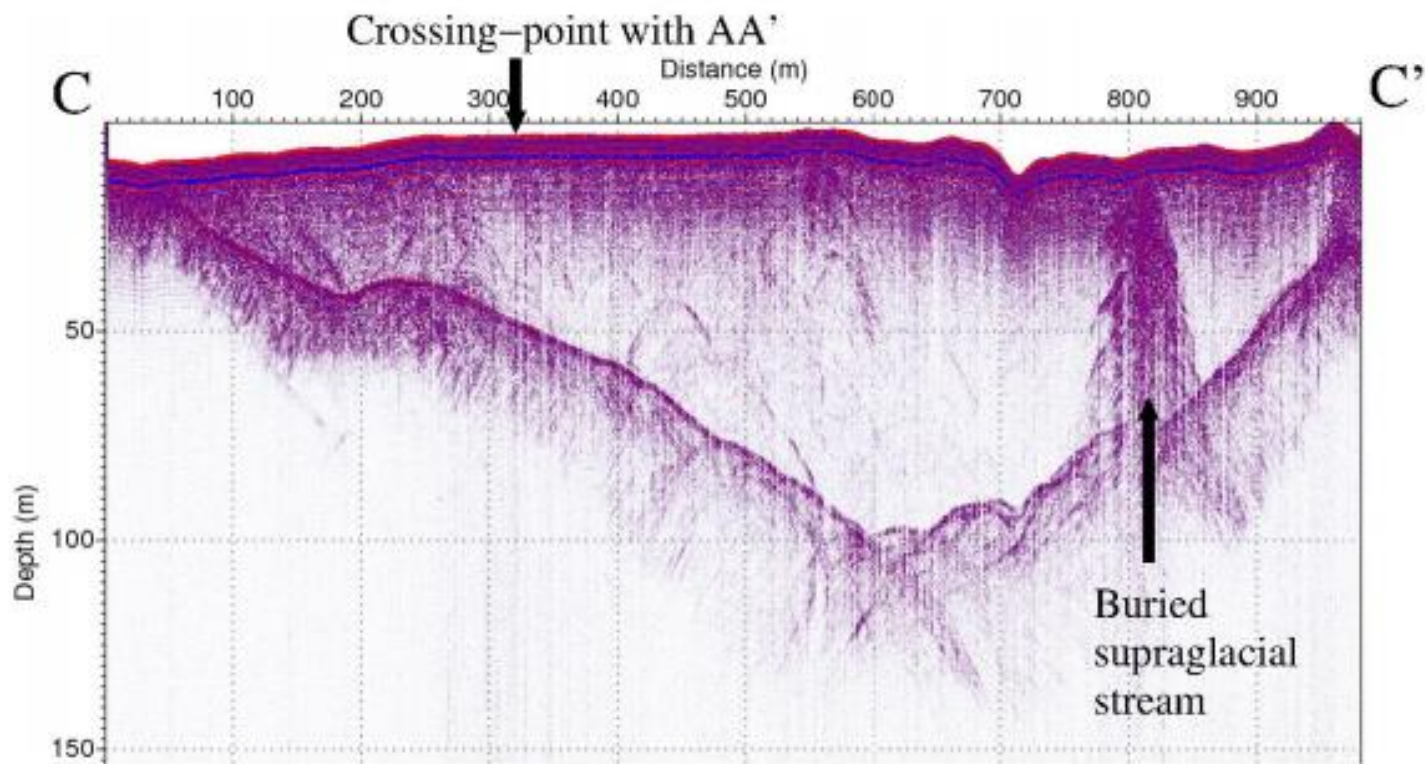
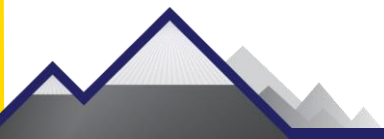


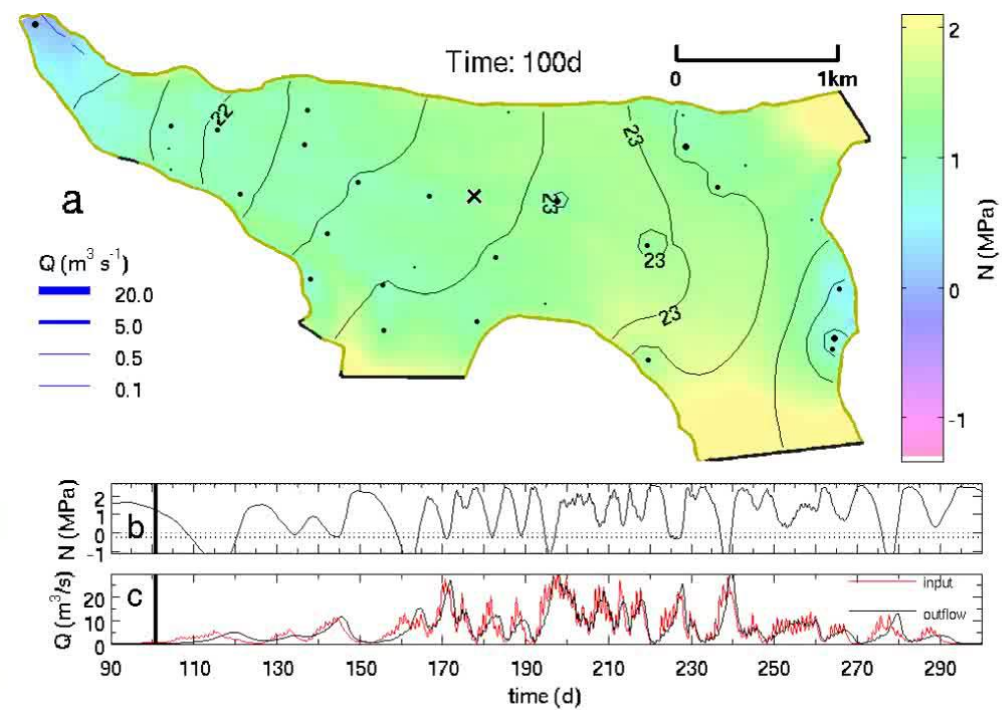
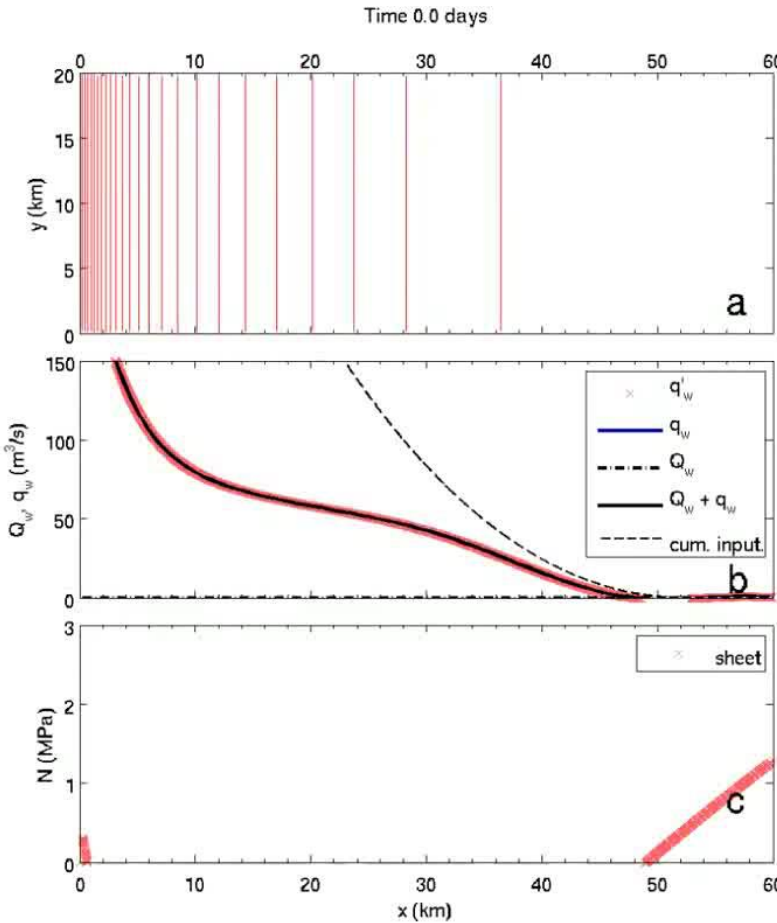
Fig. 7. Radargram CC' acquired across the glacier tongue with 100 MHz antennas (non migrated).



Tracer Tests – Subglacial Hydrology



Modelling Subglacial Hydrology





LIDAR (Spaceborne/Terrestrial)

- near-infrared Laser scanning
- Expensive + heavy



Figure 2. TLS survey of St. Annafirn in September 2014 with the *Riegl VZ[®]-6000* terrestrial laser scanner.

Fischer et al, TC (2016)



UAV – High Resolution Optical Data

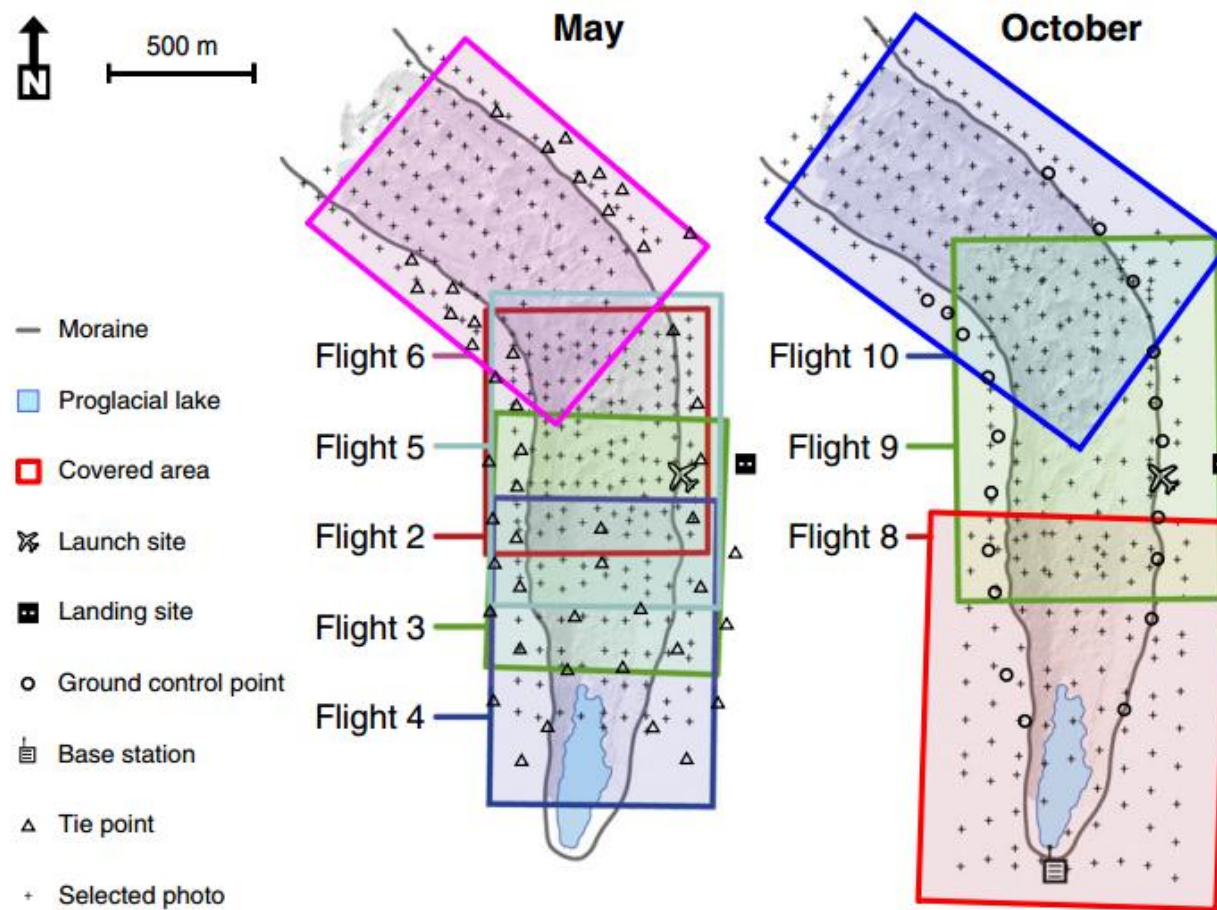


Fig. 3. Overview of the study area, approximate coverages of the successful flights, positions of the selected images and locations of the ground control points (GCP) and tie points.



DEM – Elevation Change - Velocity

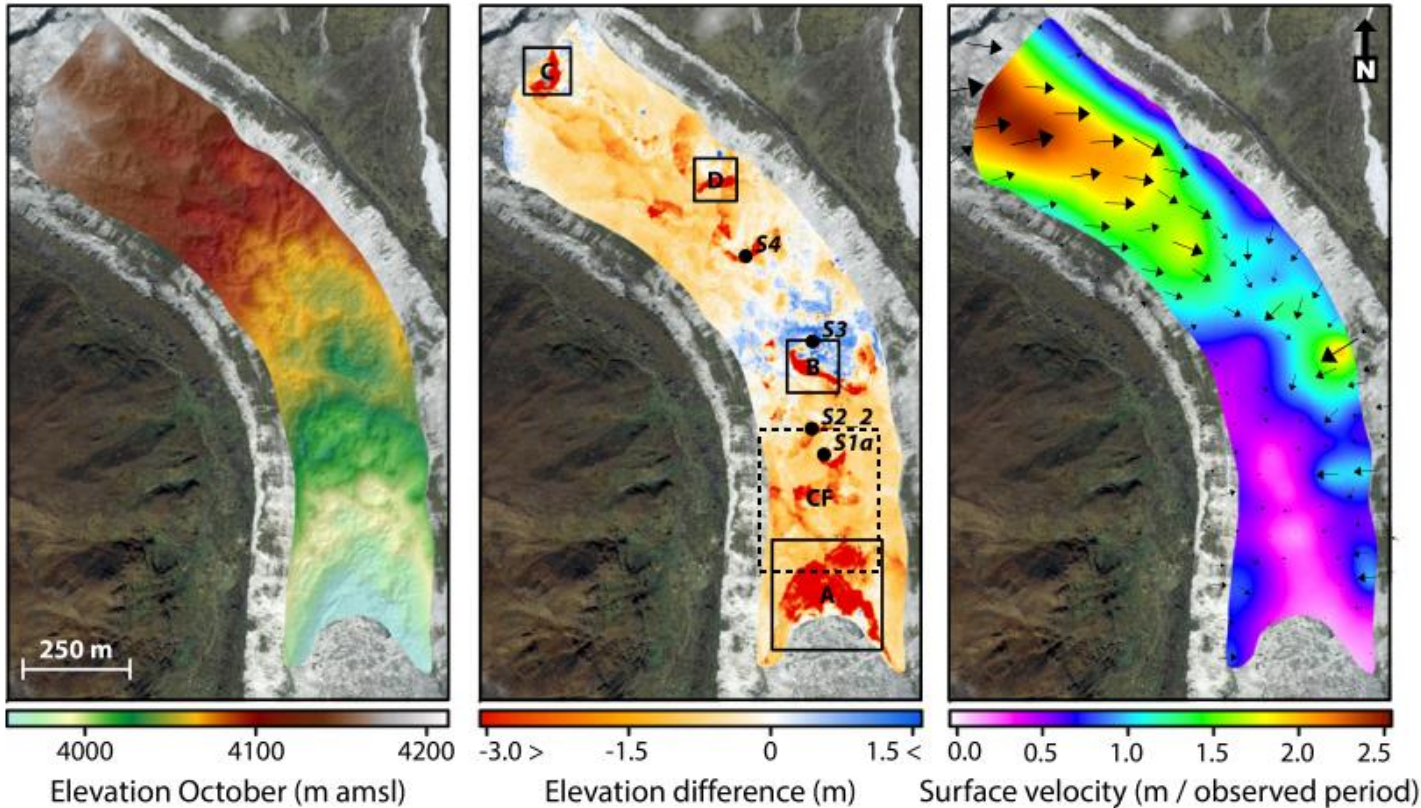


Fig. 5. Digital elevation model in October 2013 (left panel), changes in elevation between May and October 2013 (middle panel), and the derived surface velocity and direction of flow (right panel). The middle panel shows the locations of the ablation stakes and the extents of the panels of Fig. 7 (solid boxes) as well as the extent in Fig. 8 (dashed box).

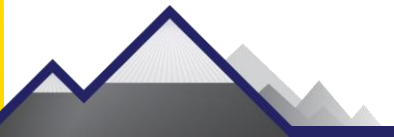


... Fieldwork!



Topics

- Why do Glaciers matter?
- Theory
- Field Methods
- Remote Sensing of Glaciers
- Modelling – *Case Studies*





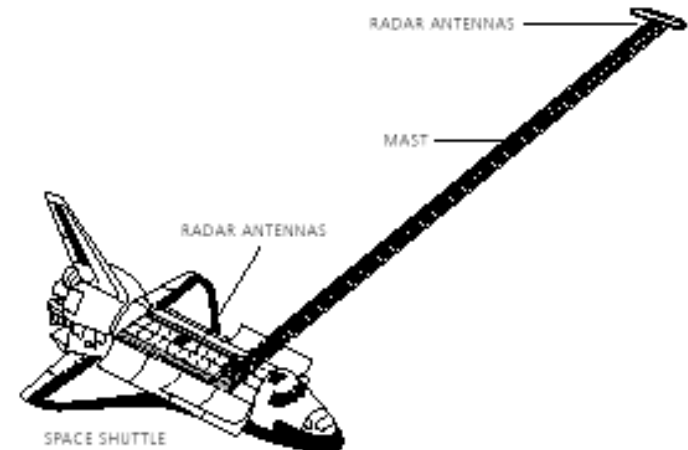
Satellites

- DEMs / Altimetry
 - Radar: SRTM (90 m), TanDEM-X (12 m)
 - IR: ASTER (30 m)
 - Optical: ALOS-PRISM, SPOT, Pleiades, CartoSat, WV ...
 - Radar Altimetry: CryoSat-2
 - Laser Altimetry: ICESat
- Velocity Data (Optical, Sentinel)
- Thermal Data (Landsat, ASTER)
- Panchromatic Imagery

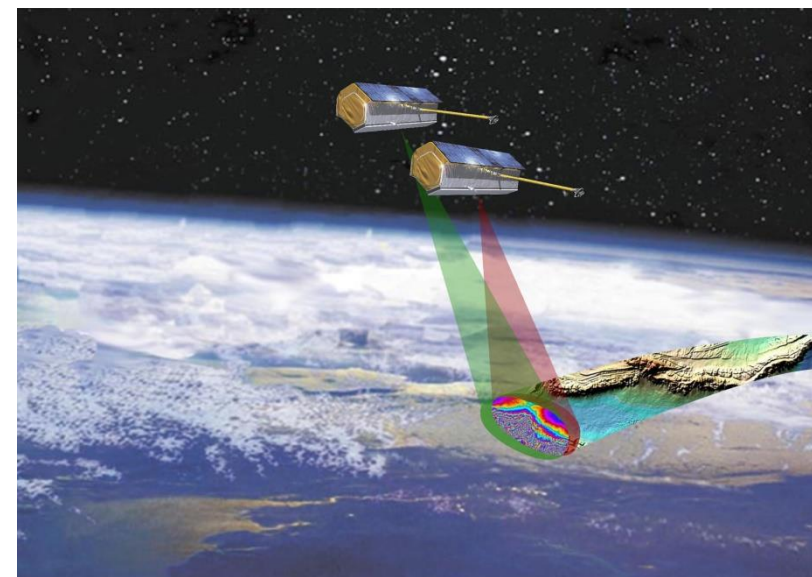


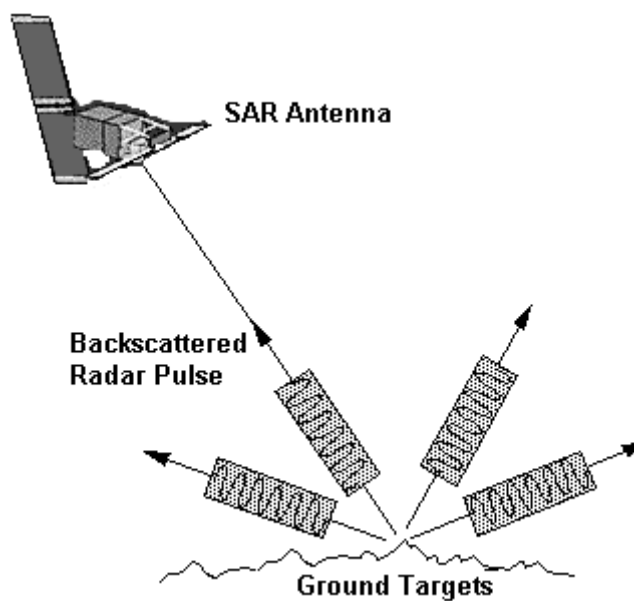
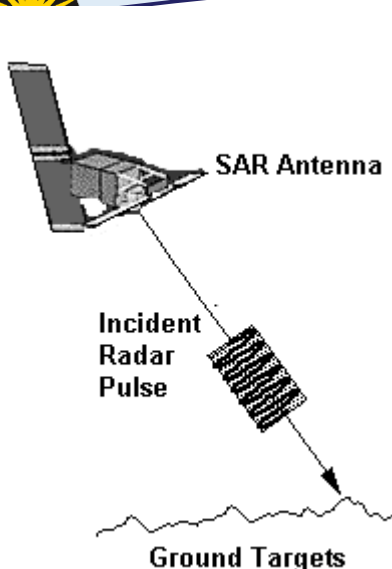
Radar

- SRTM – single mission 2000



- TanDEM-X - ongoing





- Clouds
- Ice Penetration
- Soil moisture content
- Shading

DEM^s from Orthoimagery

- bi- or tri-stereo image sampling
- commercial/open source software for processing
- GCPs essential

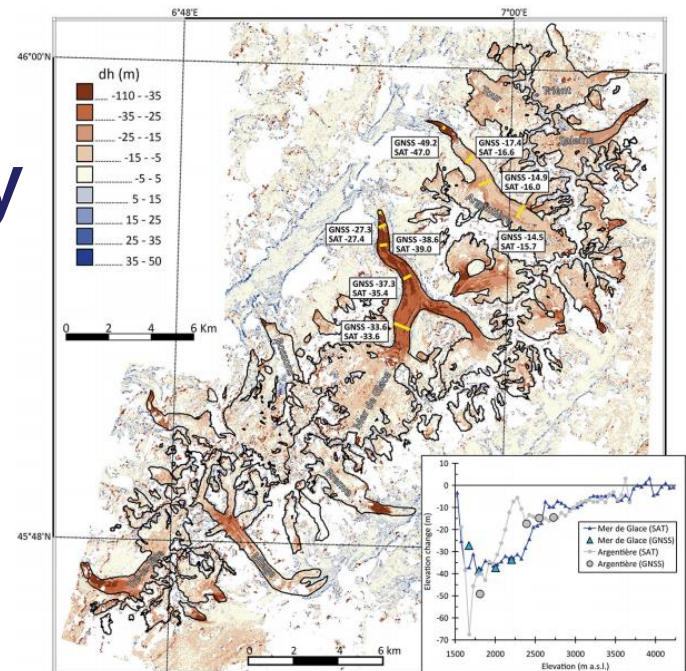
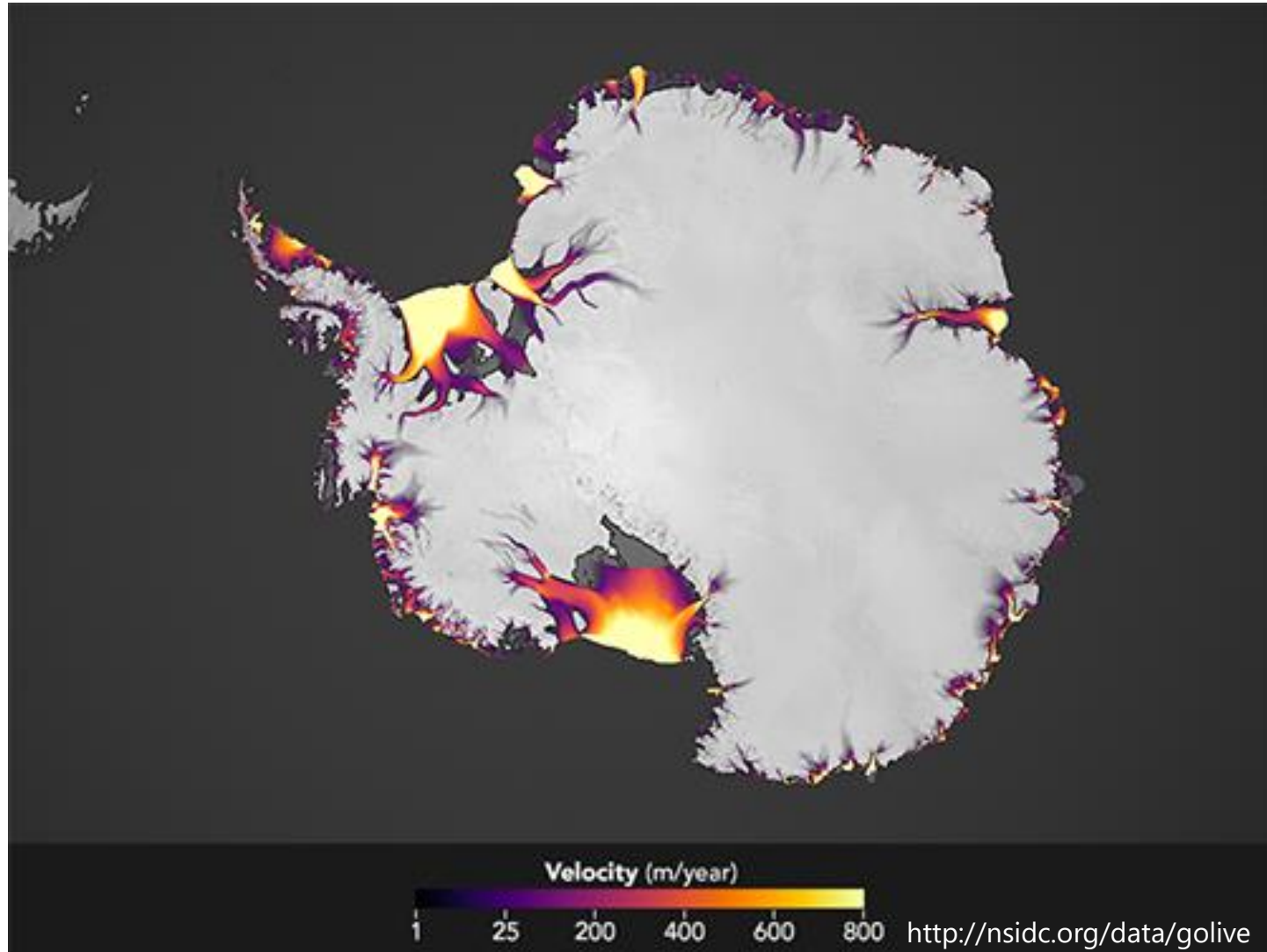


Figure 8. Elevation differences between the SPOT 5 DEM from 19 to 23 August 2003 and Pléiades DEM from 19 August 2012 over the Mont-Blanc area. In yellow, the location of the transverse profiles where elevations are measured every year using differential GNSS. The field (noted GNSS) and satellite (SAT) 2003–2012 elevation differences averaged along these profiles are indicated. Inset: satellite-derived (SAT, small symbols) and field (GNSS, large symbols) elevation changes as a function of altitude for the Mer de Glace (blue) and the Argentière (grey) glaciers. Large symbols correspond to the field measurements.



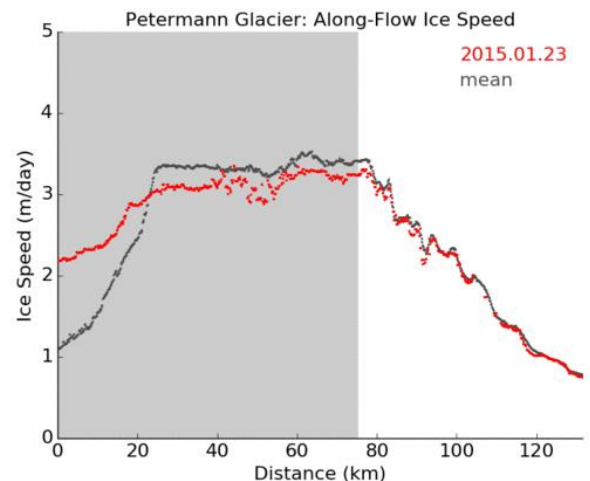
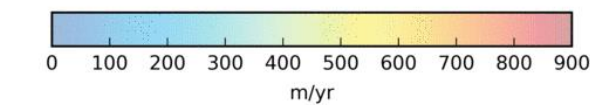
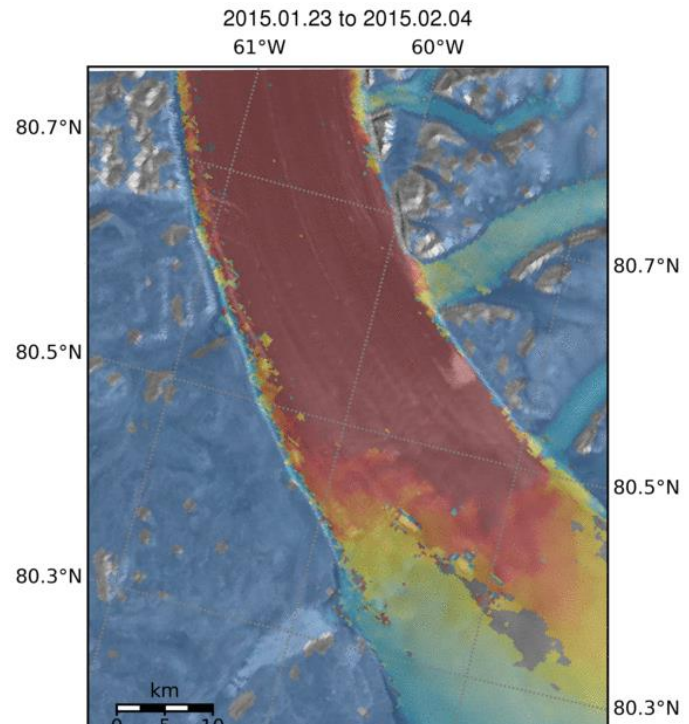


Velocity Fields – Coarse Resolution





Velocity Fields – High Resolution



Sentinel Satellites (ESA)

Thermal Data - ASTER

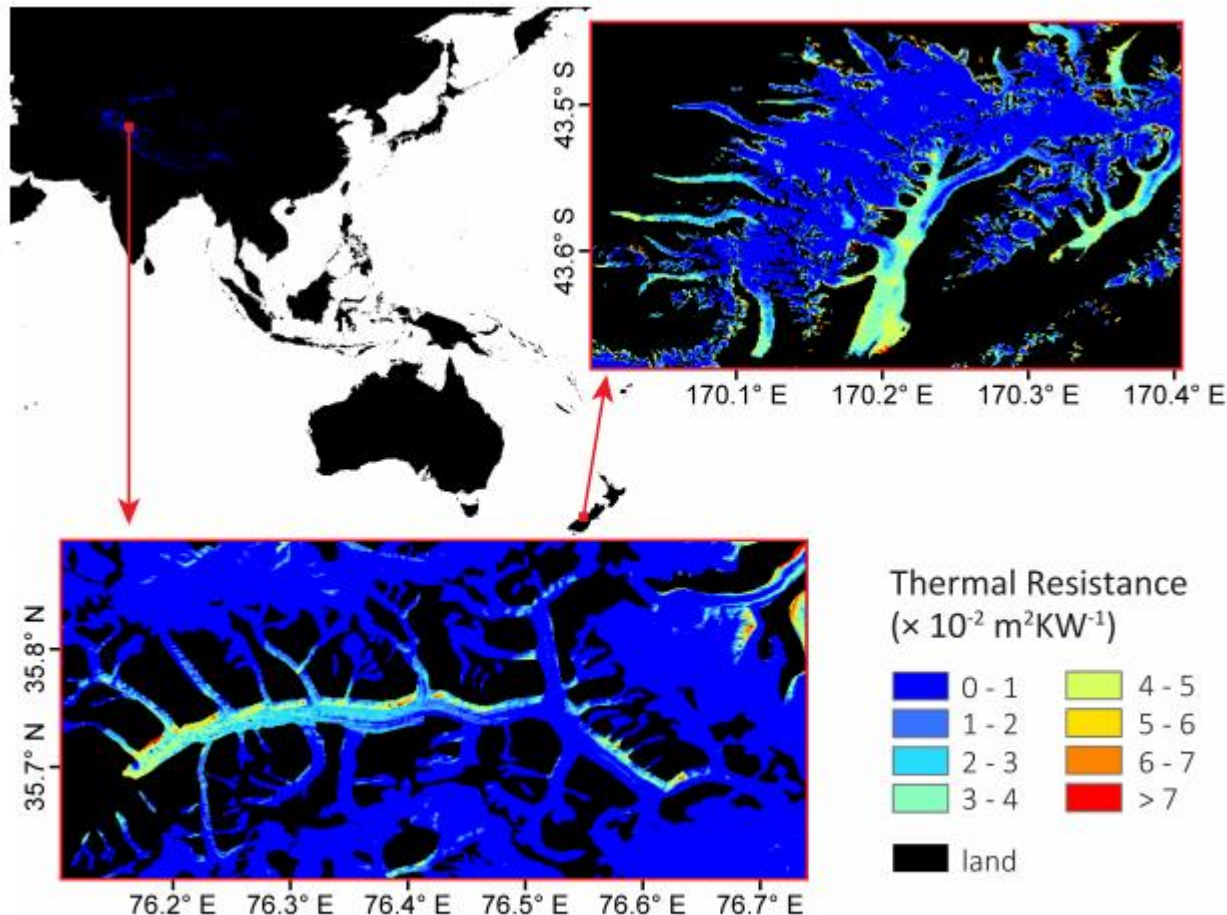
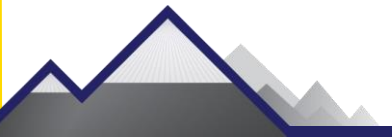


Figure 3: Thermal resistance in two regions: (a) Baltoro Glacier in Pakistan and (b) Southern Alps in New Zealand.



Panchromatic and Optical Imagery

- Landsat, ASTER, Optical
- Identifying Glacier Features
 - Crevasses
 - Ponds, Ice Cliffs
 - Moraines
- Identify Changes in Time (Seasonality)



a

Landsat TM, ETM+ Radiance (b)

1. Atmospheric correction (LandCor/6S)
2. Cloud mask (Fmask 3.2.1)
3. Shadow mask
4. Snow mask ($\text{NDSI} > 0.45$)

Masked scene (c)

5. Slope $< 30\%$
6. $\text{BR24} > 1.2$ or $\text{NDWI} > 0.3$
 $\text{BR45} < 3.5$

Water seeds (d)

7. Morph. 'close', 'fill', and segmentation
8. Object $\text{BR24} > 1.2$
Object $\text{BR45} < 3.5$
Object $\text{BT} > 273$
9. Clip to glacier outlines

Supraglacial Ponds (e)

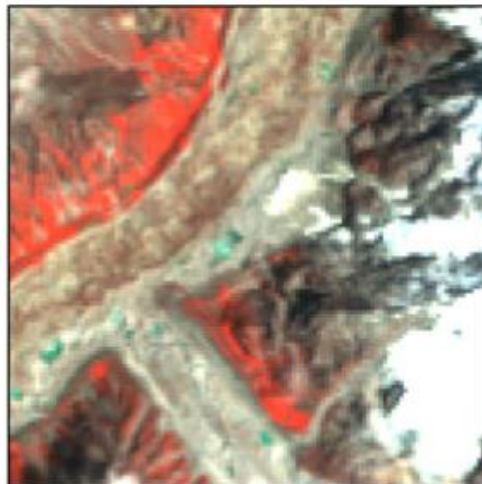
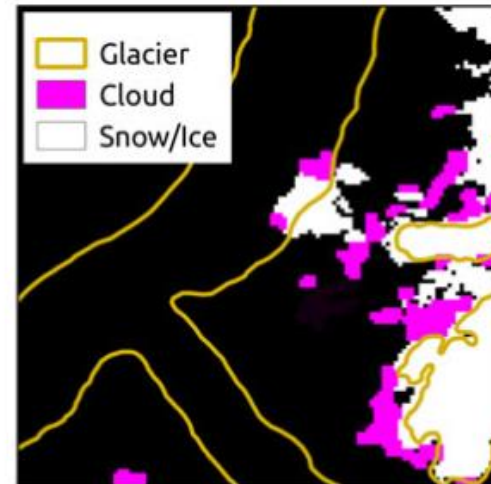
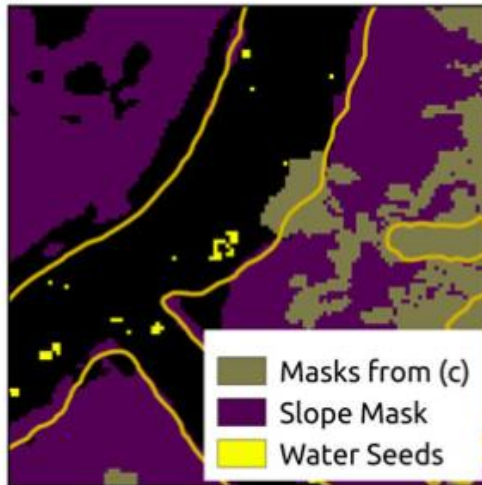
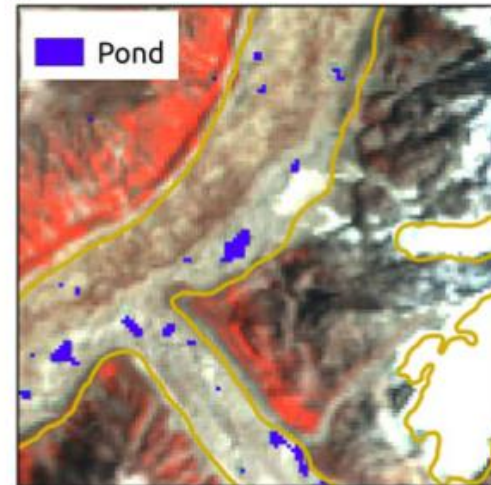
b**c****d****e**

Fig. 3. (a) Processing workflow for supraglacial pond classification, with intermediate steps shown in insets (b)–(e). (b) Subset of Landsat TM false-color composite for 19 August 2009 after Landcor/6S processing. (c) Cloud, snow/ice and shadow (not shown) masks determined by subroutines, showing some difficulty with cloud identification. (d) Slope mask and determination of high-probability water seeds. (e) Pond cover output after image morphological operations and reclassification.



Kraaijenbrink et al., RSE (2016)

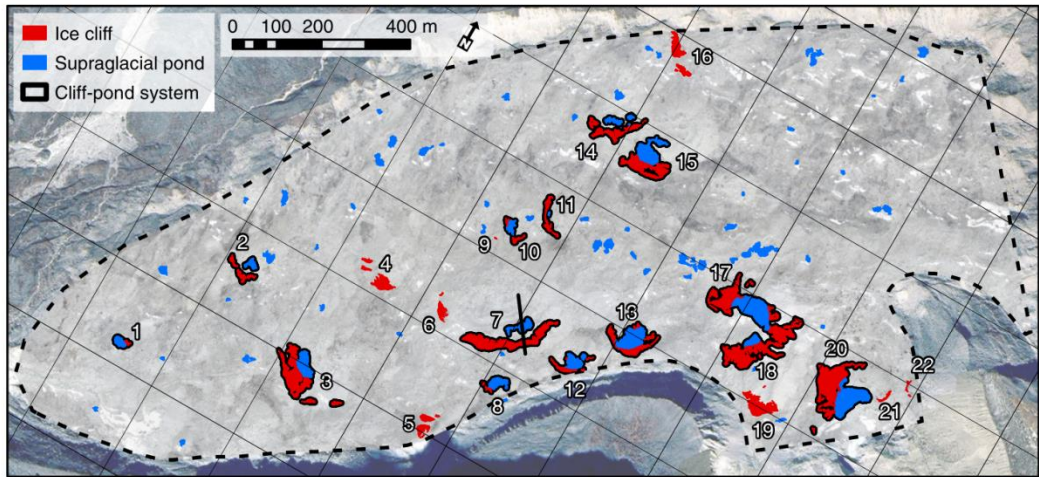
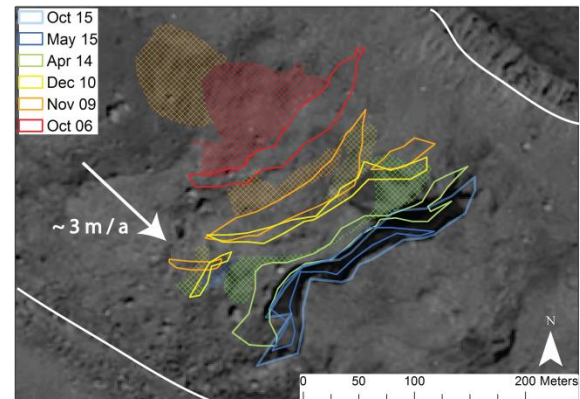
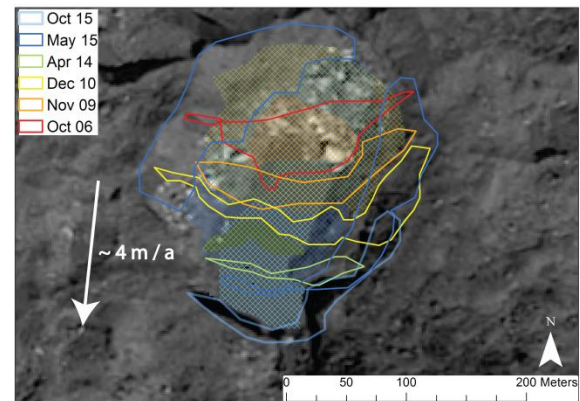


Fig. 5. Ice cliffs and supraglacial ponds on Langtang Glacier as classified on the May 2014 UAV imagery by OBIA. Annotation shows the numbered, grouped cliff objects that belong to the same cliff system. Additionally, cliff-pond systems are outlined with black. The extent of the imagery and elevation subset used as classification input is delineated by the dashed line. The black line at cliff 7 denotes the location of the profile shown in Fig. 8.

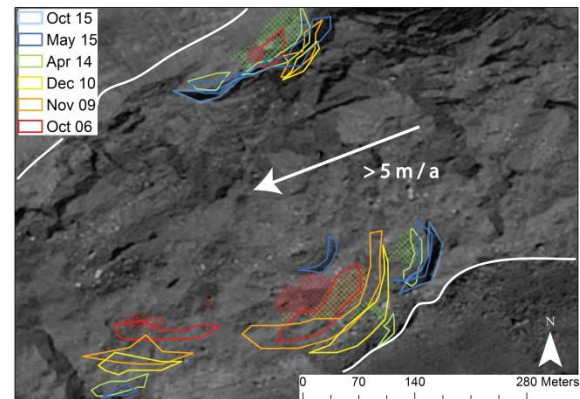
a - Lateral Cliff - Pond System (Lirung Glacier)



b - Circular Cliff - Pond System (Langtang Glacier)



c - Longitudinal Cliff - Pond Systems (Langshisha Glacier)





Remote Sensing Study - Classical

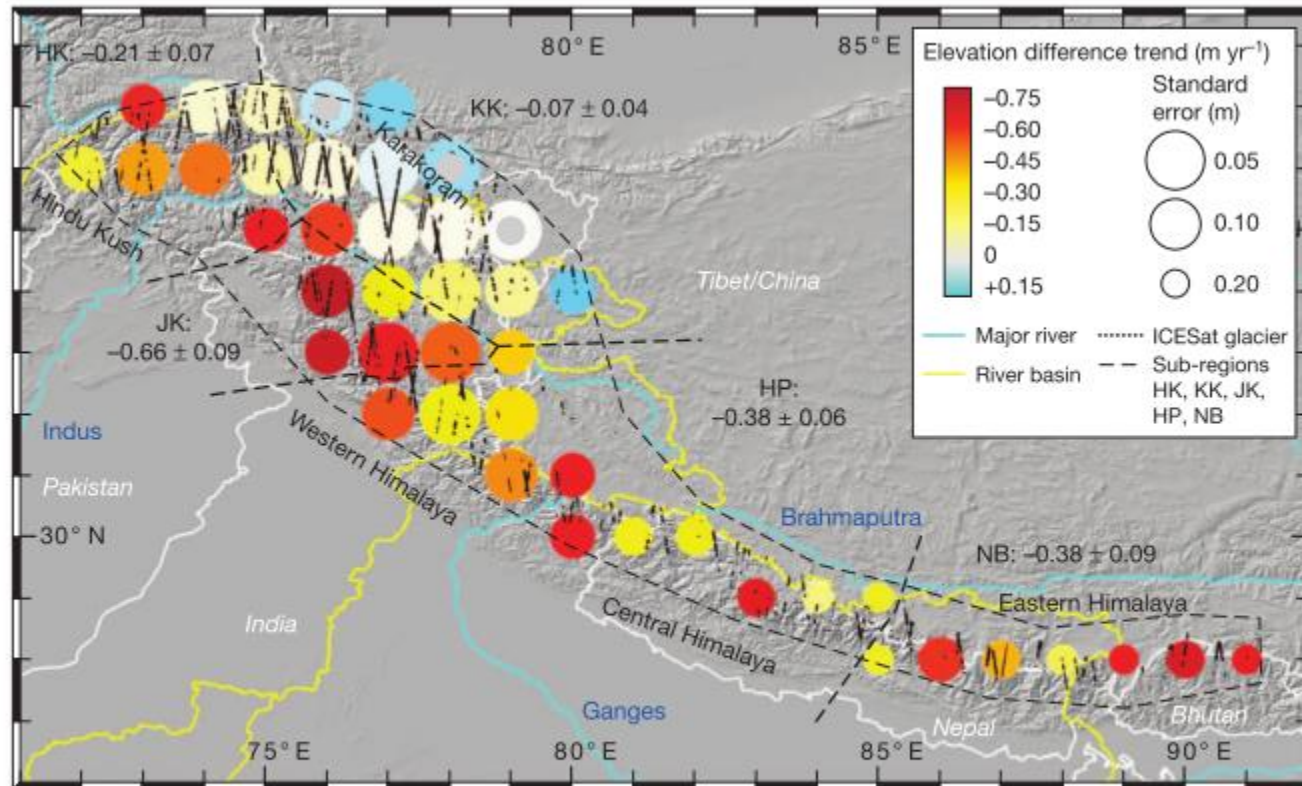


Figure 1 | Study region and trends of elevation differences between ICESat and SRTM over 2003–08. Data are shown on a 1° grid with overlapping rectangular geographic averaging cells of 2° × 2°. Trends are based on autumn ICESat acquisitions. The mean trends for each subregion are given in metres

per year. Only ICESat footprints over glaciers are indicated (the glacier mark is shown in Supplementary Fig. 1). Trends for all cells (coloured data circles) are statistically significant except for three cells in the Karakoram that are indicated with grey centres. Errors are one standard error (1 s.e.).



Remote Sensing Study – the Future

Satellite Images of Rotug Glacier



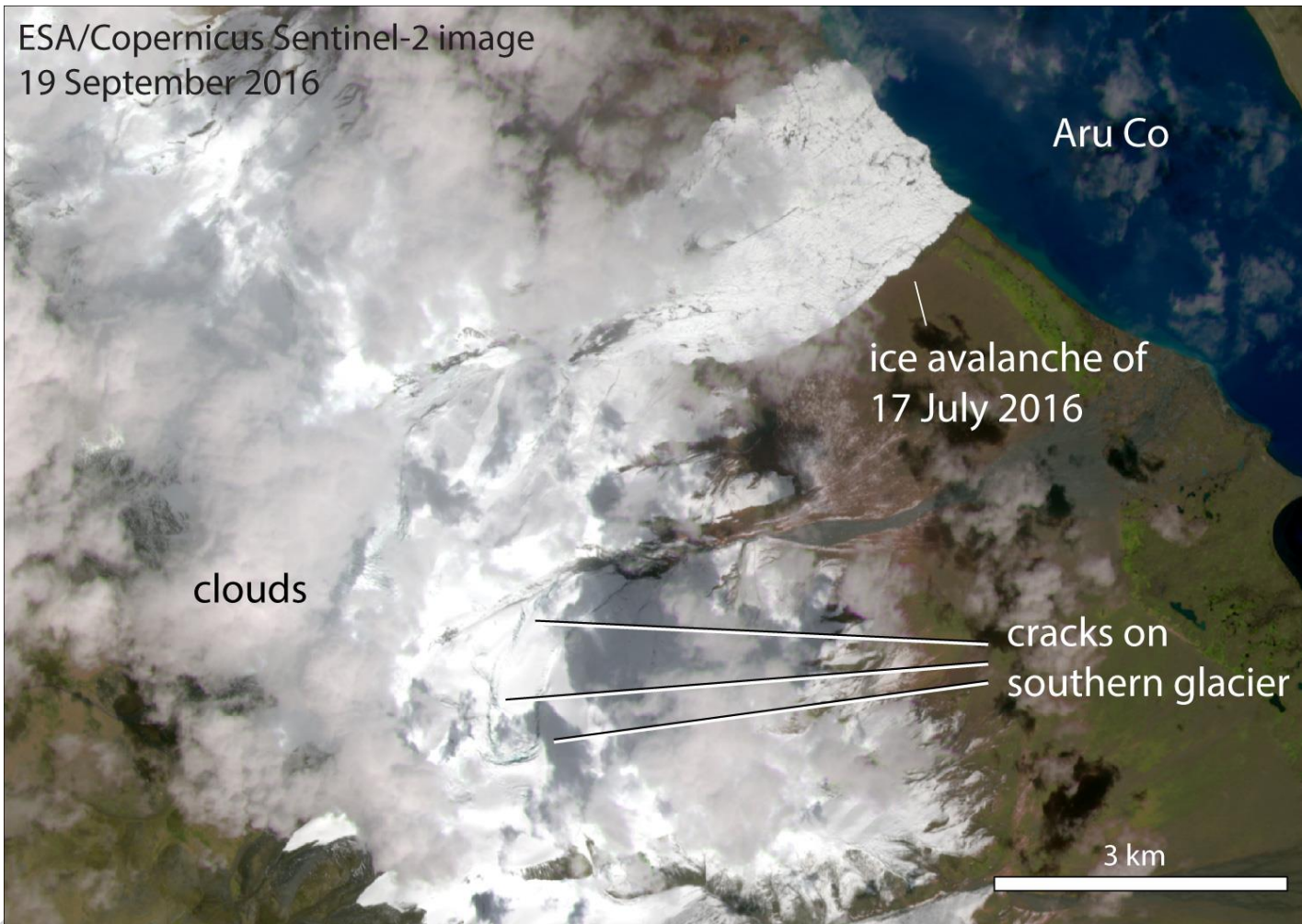
Before



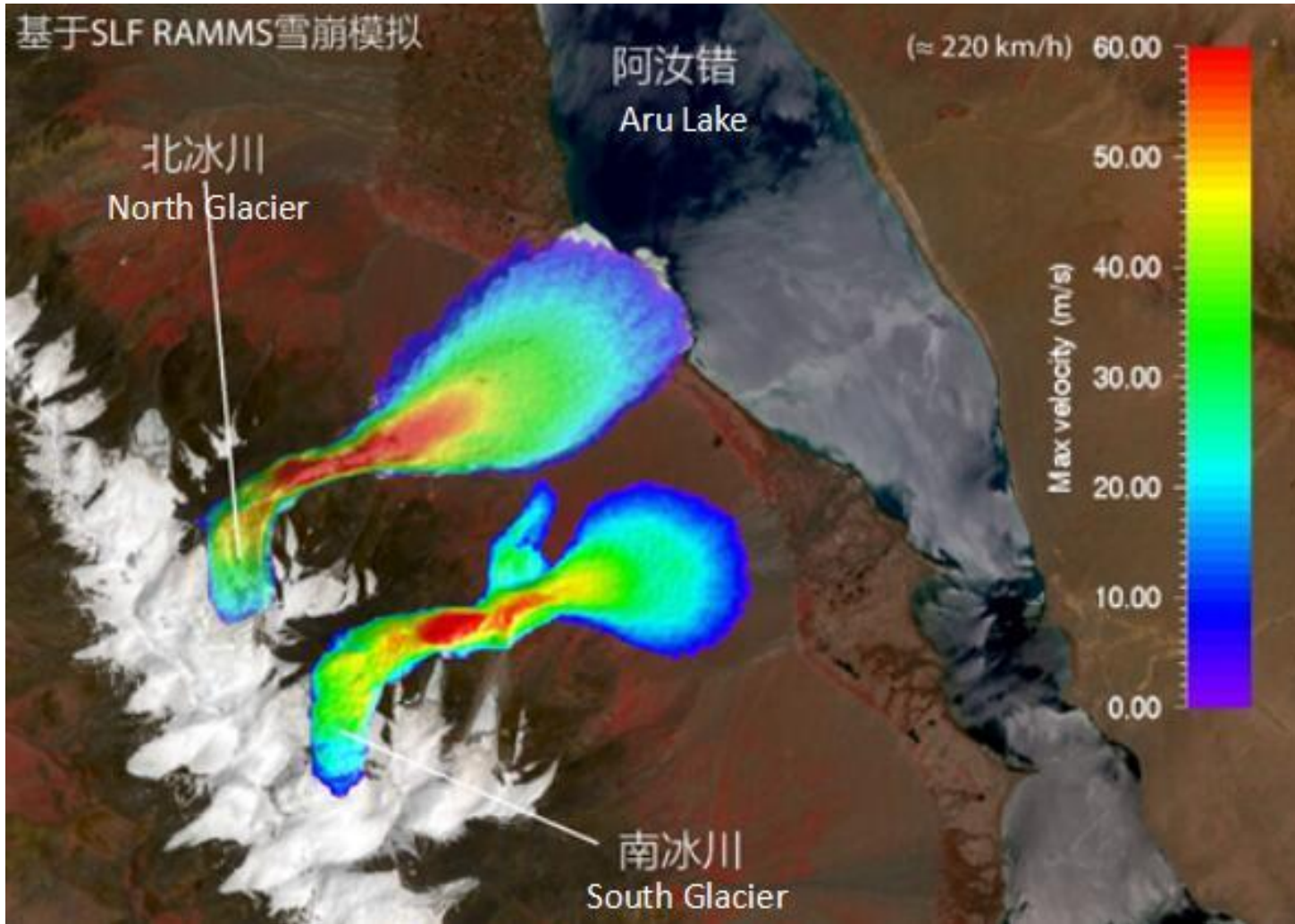
After



High Resolution Imagery of Fractures



Prediction of Glacier Collapse

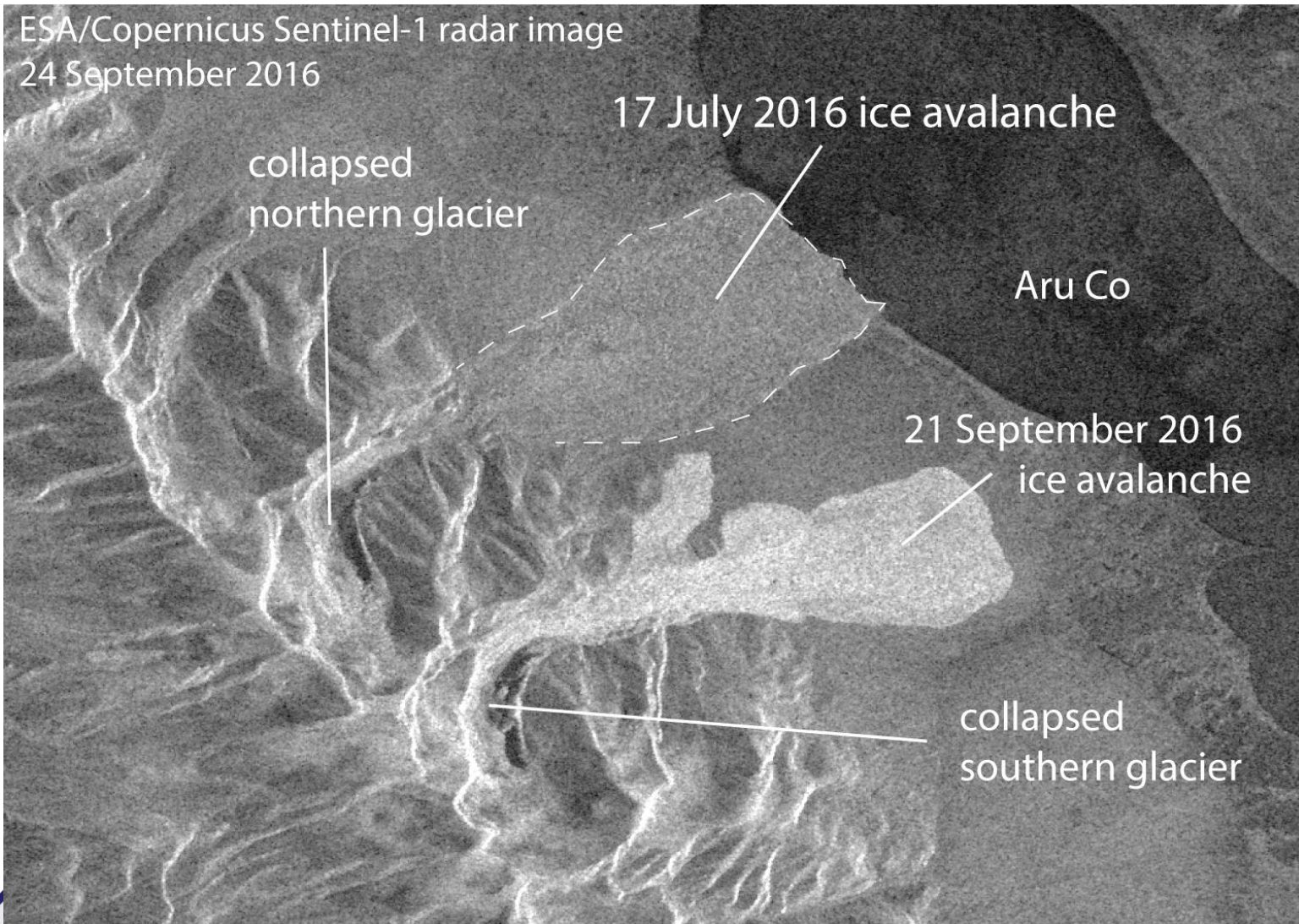




Collapse of second glacier

ESA/Copernicus Sentinel-1 radar image

24 September 2016





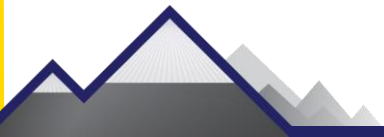
Topics

- Why do Glaciers matter?
- Theory
- Field Methods
- Remote Sensing of Glaciers
- Modelling - *Case Studies*



Case Study Local - Langtang

- Ragettli et al. (2016). Heterogeneous glacier thinning patterns over the last 40 years in Langtang Himal. *The Cryosphere*
- Ragettli et al. (2015). Unraveling the hydrology of a Himalayan catchment through integration of high resolution in situ data and remote sensing with an advanced simulation model. *Advances in Water Resources*, 78(0), 94–111



1 – Research Question and Study Site

*Heterogeneous
glacier thinning
patterns over the
last 40 years in
Langtang Himal*

Ragettli et al., TC (2016)

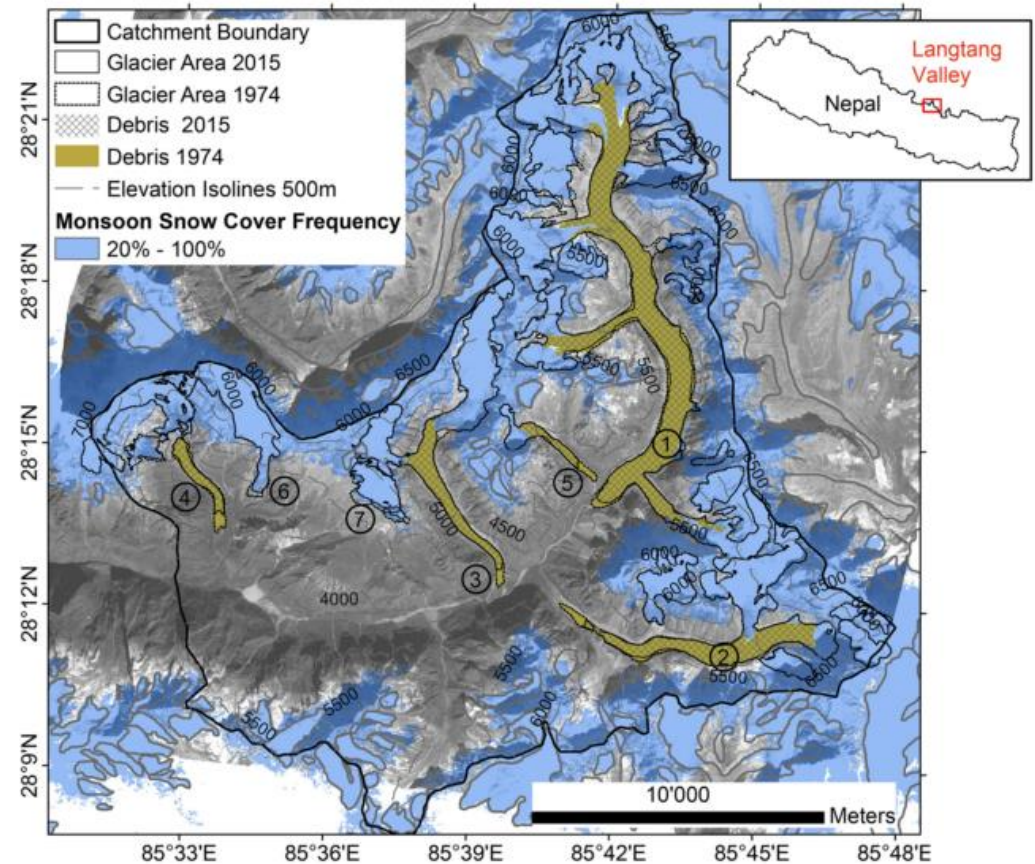


Figure 1. Map of the upper Langtang catchment. The numbers on the map correspond to the glaciers listed in Table 1. Monsoon snow-cover frequency is based on Landsat 1999 to 2013 land cover classifications (Miles et al., 2016b). The 1974 glacier area (dotted lines) is shown for the seven studied glaciers only.



2 – Study Data

Table 2. Remote-sensing data used.

Sensor	Date of acquisition	Stereo mode (<i>b / h</i> ratio)	Spatial/radiometric resolution	Role
Hexagon KH-9	23 Nov 1974	Stereo (0.4)	6–9 m/8 bit	DEM differencing, glacier outlines
Cartosat-1	15 Oct 2006	Stereo (0.62)	2.5 m/10 bit	DEM differencing, glacier outlines
Cartosat-1	9 Nov 2009	Stereo (0.62)	2.5 m/10 bit	DEM differencing, velocities, glacier outlines
ALOS PRISM	3 Dec 2010	Tri-stereo (0.5)	2.5 m/8 bit	DEM differencing, velocities, glacier outlines
SPOT6	21 Apr 2014	Tri-stereo (0.5)	1.5 m/12 bit	DEM differencing, glacier outlines
WorldView-2	2 Feb 2015	Stereo (0.5)	0.46 m/11 bit	DEM differencing
WorldView-3	22 Feb 2015	Stereo (0.5)	0.31 m/11 bit	DEM differencing
SPOT7	7 May 2015	Tri-stereo (0.64)	1.5 m/12 bit	DEM differencing, glacier outlines
SPOT7	6 Oct 2015	Tri-stereo (0.68)	1.5 m/12 bit	DEM differencing
Pléiades	1 and 9 Nov 2014	Across track stereo (0.4)	0.5 m/12 bit	Basis for georectification

3 – Methodology and Uncertainty Analysis

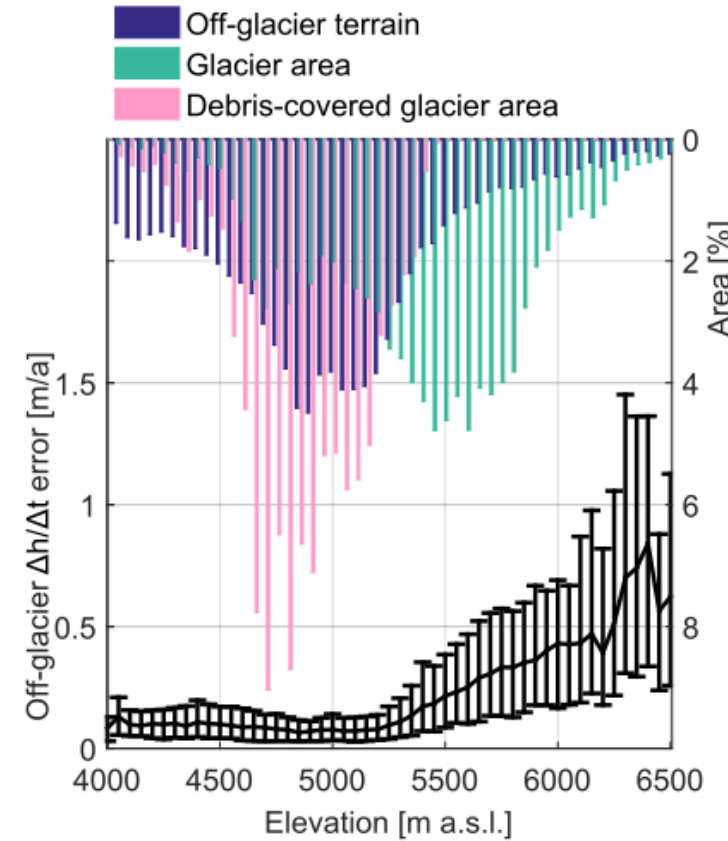


Figure 3. Off-glacier elevation change error ($\Delta h / \Delta t$) per 50 m elevation band. The black line represents the median error in the ensemble of six $\Delta h / \Delta t$ maps. Error bars represent 95 % confidence intervals. The color bars represent hypsometries of glacier area, off-glacier area and debris-covered glacier areas, respectively.



4 - Results

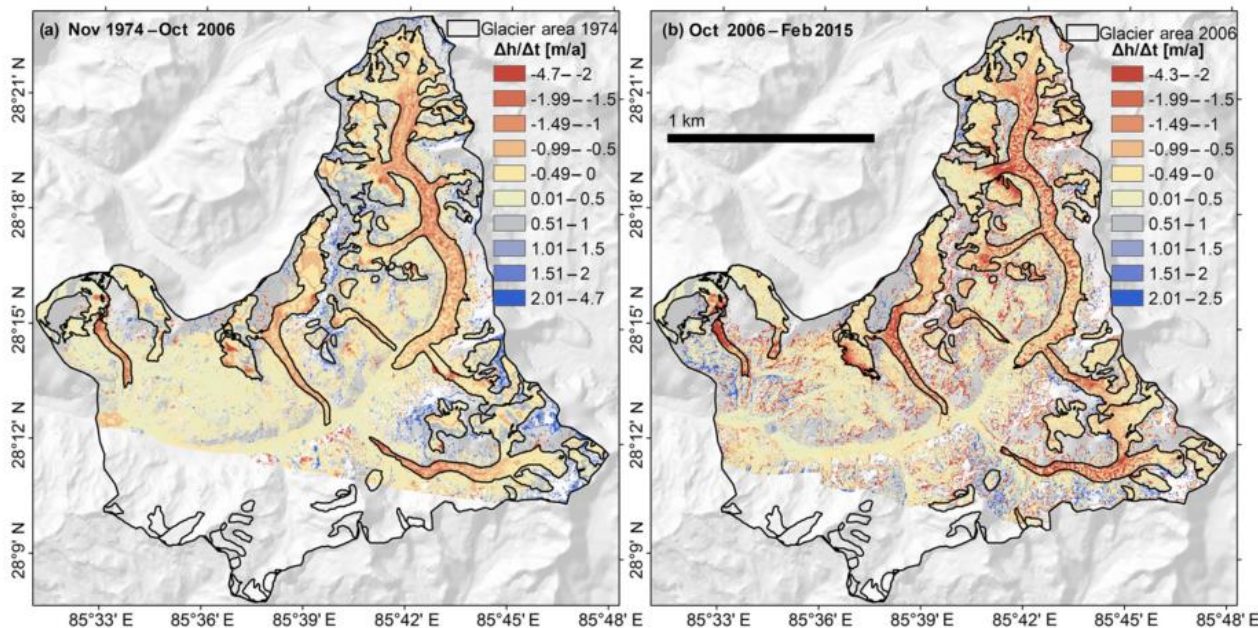


Figure 4. Elevation change rates ($\Delta h / \Delta t$) derived from (a) Hexagon November 1974 and Cartosat-1 October 2006 DEMs and (b) Cartosat-1 October 2006 and WorldView February 2015 DEMs.



4 - Results

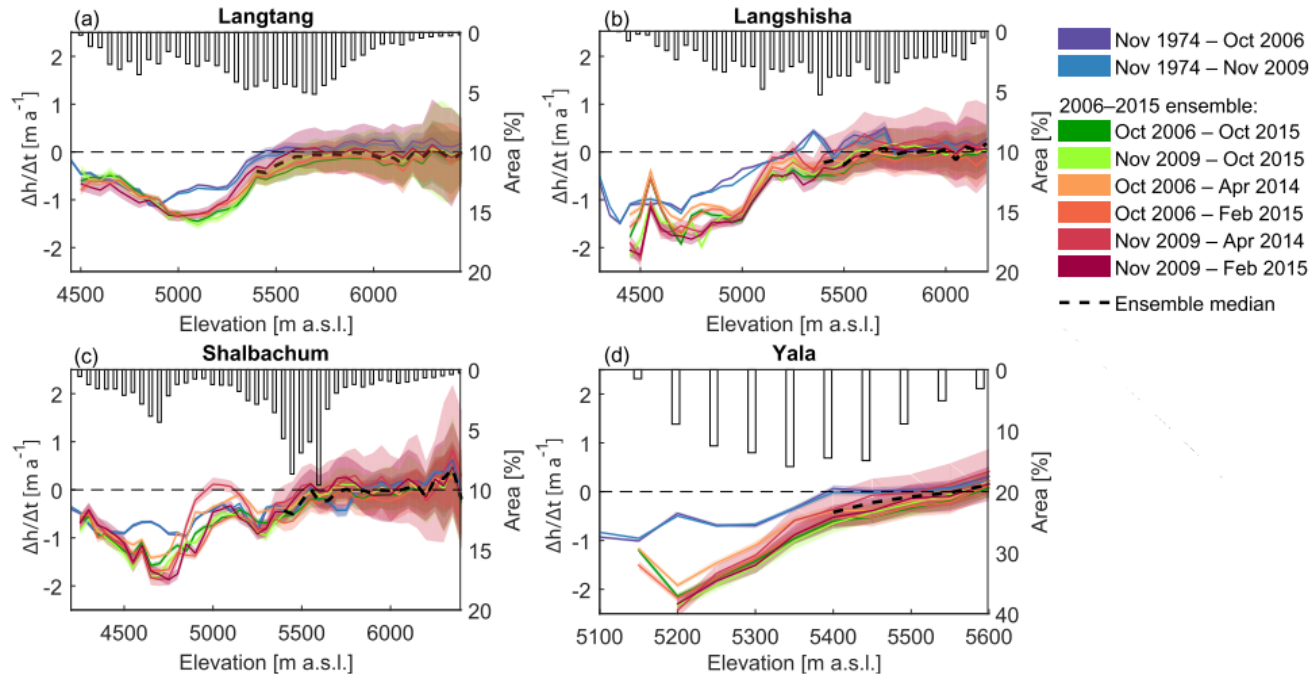


Figure 10. Altitudinal distribution of mean annual elevation change ($\Delta h / \Delta t$) and altitudinal distribution of glacier area (%) over 50 m elevation bands of selected glaciers. Uncertainty bounds correspond to uncertainty as a function of elevation derived for each $\Delta h / \Delta t$ map individually (Fig. 3). Ensemble median values shown here are used to replace missing data in the accumulation areas of glaciers after outlier exclusion (Sect. 3.2.3). Note that the x axis ranges are different for each sub-figure.



5 – Discussion – how to interpret the results?

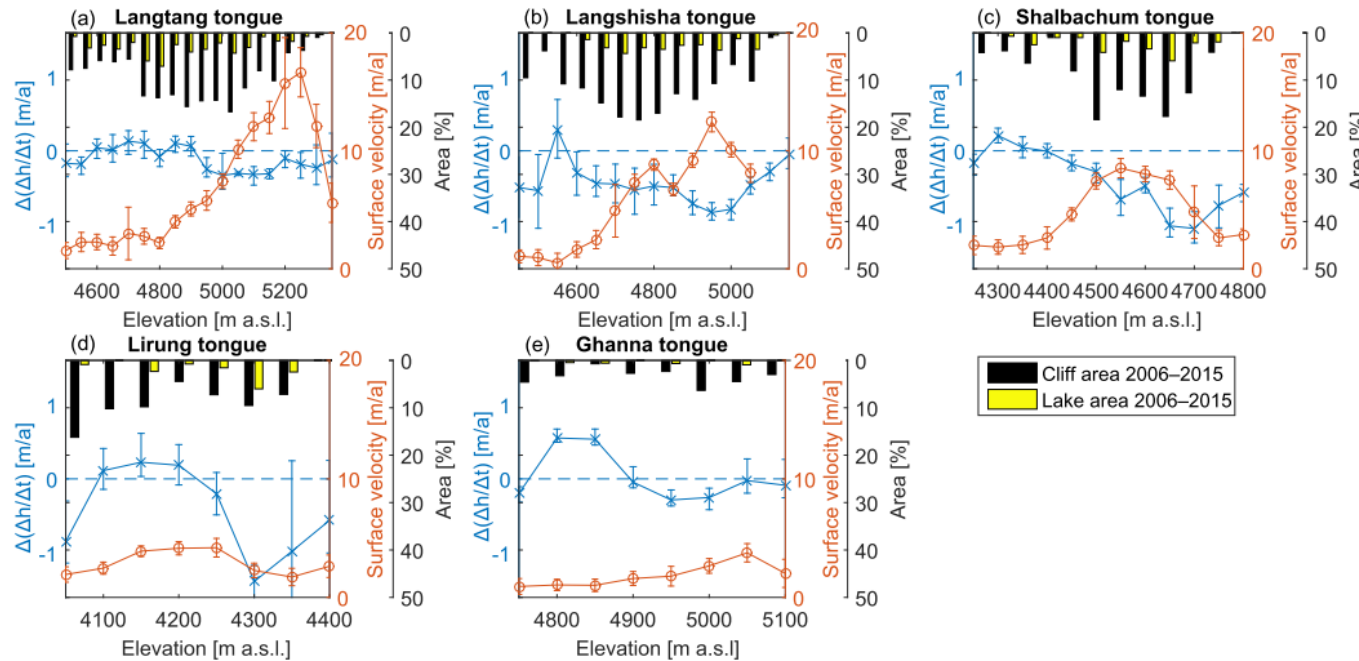


Figure 11. Altitudinal distribution of cliff and lake area fractions, glacier velocity and changes in thinning rates. Cliff and lake area is shown as % of 30 m pixels containing cliffs/lakes per 50 m elevation band, whereas the values represent the median of six available cliff and lake maps from the period 2006–2015. Glacier velocities (m a^{-1}) represent the median per 50 m elevation band of data shown in Fig. 13 and error bars represent the standard deviation in pixel values per elevation band. Changes in thinning rates ($\Delta(\Delta h / \Delta t) [\text{m a}^{-1}]$) are calculated comparing 1974–2006 and the 2006–2015 ensemble mean. Negative $\Delta(\Delta h / \Delta t)$ values represent thinning accelerations. Error bars represent the maximum variations in $\Delta(\Delta h / \Delta t)$ considering all individual periods within the 2006–2015 ensemble.

1 – Research Question and Study Site

*Unraveling the
hydrology of a
Himalayan
catchment ...*

Ragettli et al., AWW (2015)

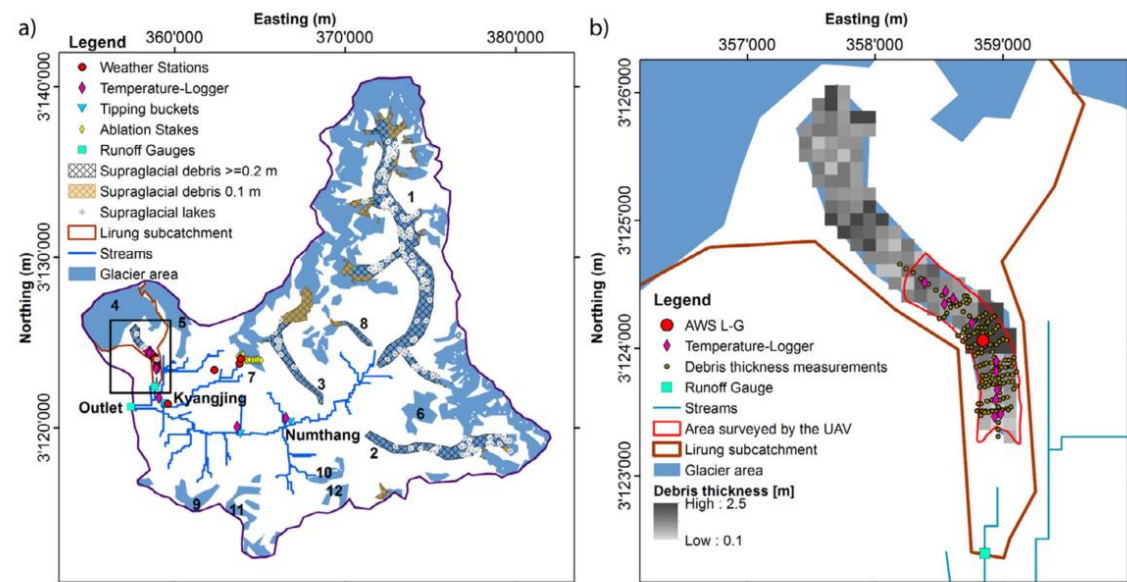


Fig. 1. (a) Map of the upper Langtang catchment showing the position of meteorological stations and streamgauges (Table 2), tipping buckets and temperature loggers, ablation stakes and Landsat ETM+ derived supraglacial lakes. The numbers on the map indicate the locations of glaciers listed in Table 1. (b) Map of the glacier tongue of Lirung Glacier. The Unmanned Aerial Survey System (UAV) range shows the area that has been mapped by airborne stereo imagery in May and October 2013. The debris thickness values within the UAV range indicate reconstructed debris thickness, and outside the UAV range the randomly sampled reconstructed debris thickness.

2 – Study Data and Methodology

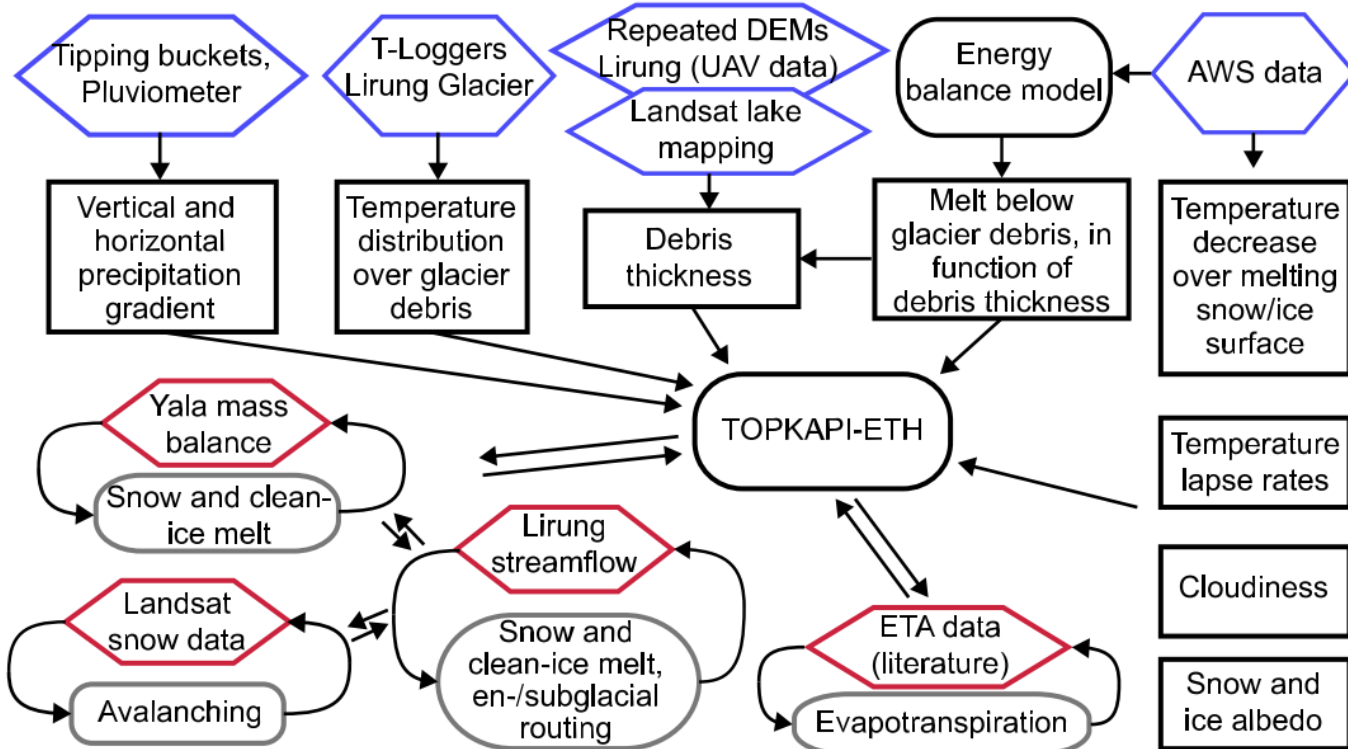


Fig. 2. Scheme of the methodology developed to estimate optimal model parameters for the upper Langtang valley making maximal use of available in situ data. Rectangular boxes represent model parameters that are directly calculated using local data (blue hexagons). Those parameters are kept fixed during the calibration of other model components – represented by gray rounded shapes – against the calibration datasets (red hexagons). (For interpretation of the references to color in this figure legend, the reader is referred to the web version of this article.)

3 – Results and Future Challenges

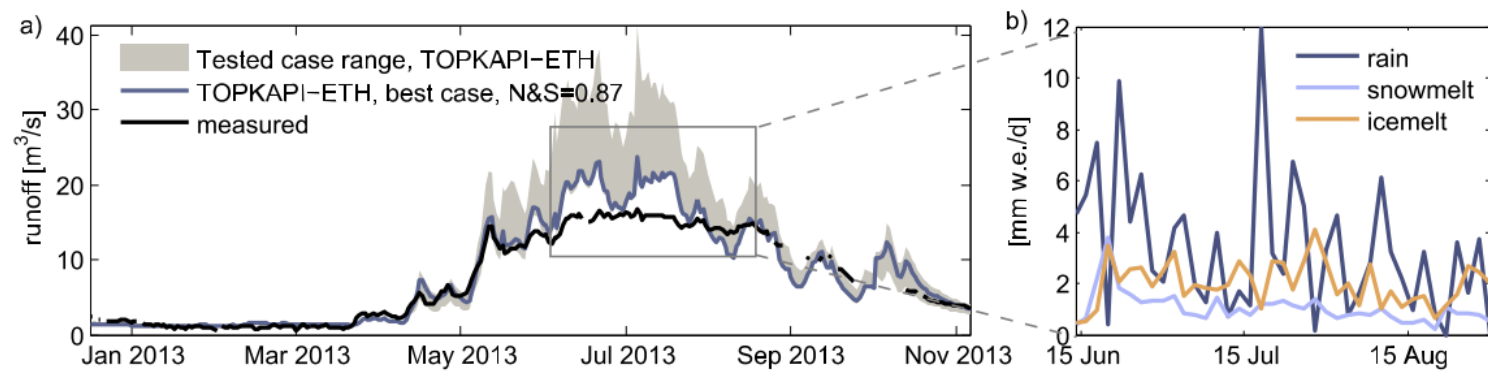


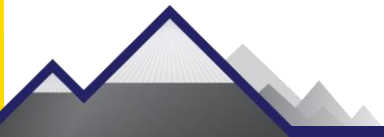
Fig. 6. (a) Simulated and measured daily runoff at Langtang Khola streamgauge. The tested case range corresponds to the model outputs simulated with the tested model setups indicated in [Table 4](#). The 'best case' corresponds to case 8 in [Table 4](#). (b) Running 72 h mean values of water balance components corresponding to case 8 model outputs.



Case Study Global – Global Glacier Mass Balance Modelling and SLR

Huss, M., & Hock, R. (2015). A new model for global glacier change and sea-level rise.

Frontiers in Earth Science, 3(September), 1–22.





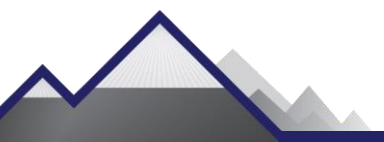
1 – Research Question and Data

TABLE 1 | Number of glaciers n and glacier area according to the Randolph Glacier Inventory (RGIv4.0) (Pfeffer et al., 2014).

Region	n (-)	Area (km 2)	SLE (mm)	Years (yr)
Alaska	26,944	86,715	45.28	2009±2
Western Canada	15,215	14,559	2.47	2004±5
Arctic Canada North	4538	104,873	67.02	1999±0
Arctic Canada South	7347	40,894	19.70	2000±6
Greenland Periphery	19,323	89,721	37.81	2001±2
Iceland	568	11,060	8.13	2000±1
Svalbard	1615	33,922	19.93	2007±6
Scandinavia	2668	2851	0.36	2001±2
Russian Arctic	1069	51,592	30.68	2002±3
North Asia	4403	3430	0.40	1970±19
Central Europe	3920	2063	0.28	2003±5
Caucasus	1386	1139	0.15	2000±15
Central Asia	46,543	62,606	9.99	1970±8
South Asia West	22,822	33,859	7.56	2000±11
South Asia East	14,095	21,799	2.99	2000±17
Low Latitudes	2863	2346	0.20	2002±3
Southern Andes	16,046	29,333	13.00	2000±0
New Zealand	3537	1162	0.15	1978±0
Antarctic	2752	132,867	107.90	1989±15
GLOBAL	197,654	726,792	374.00	

Ice volume is calculated from the methods by Huss and Farinotti (2012), and converted to sea-level equivalent (SLE) assuming an ice density of 900 kg m $^{-3}$ and an ocean area of 3.625×10^8 km 2 . Years refer to the average satellite acquisition date for each glacier outline in the region (± 1 standard deviation).

Huss and Hock, FiES (2015)





2 - Methodology

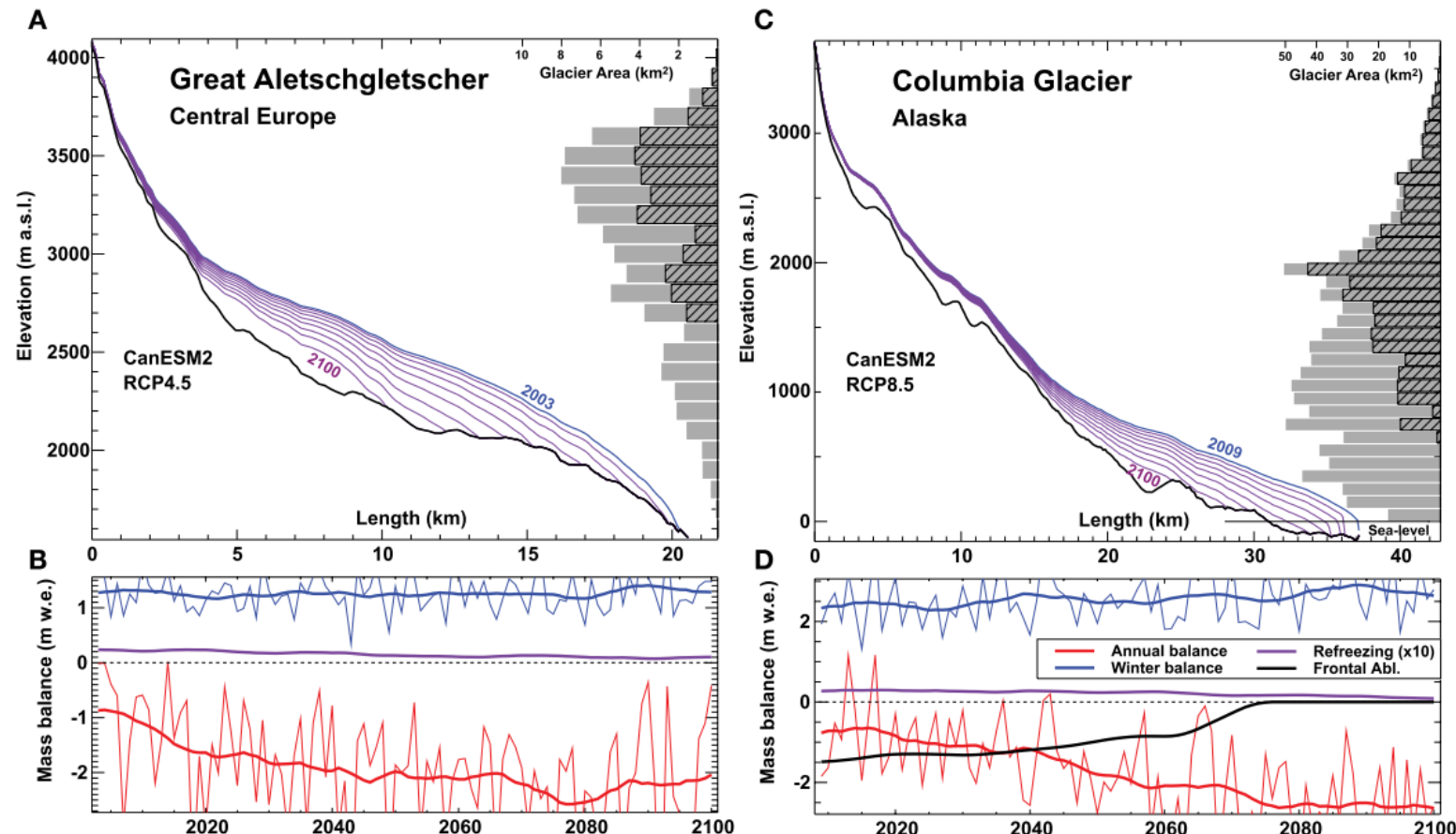
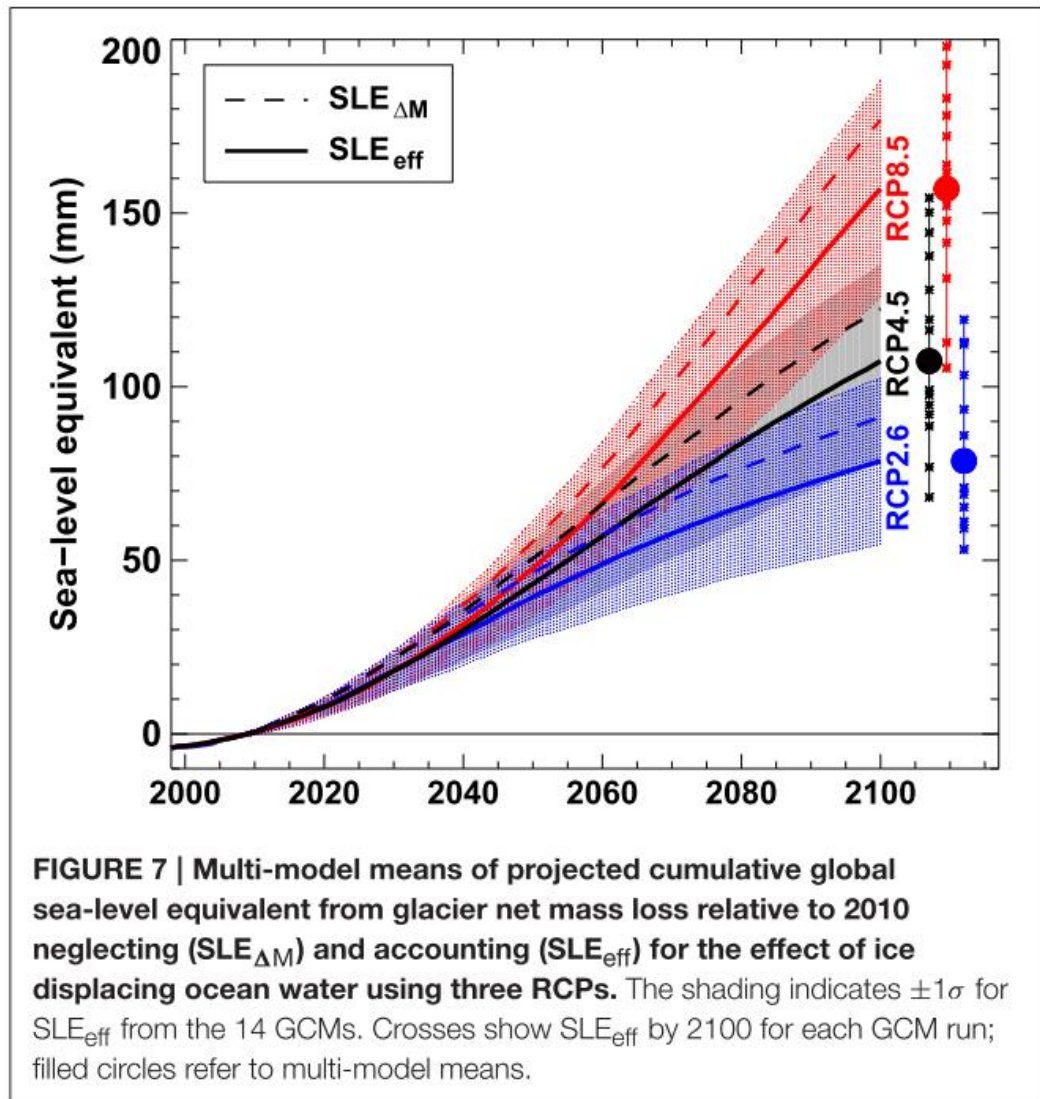
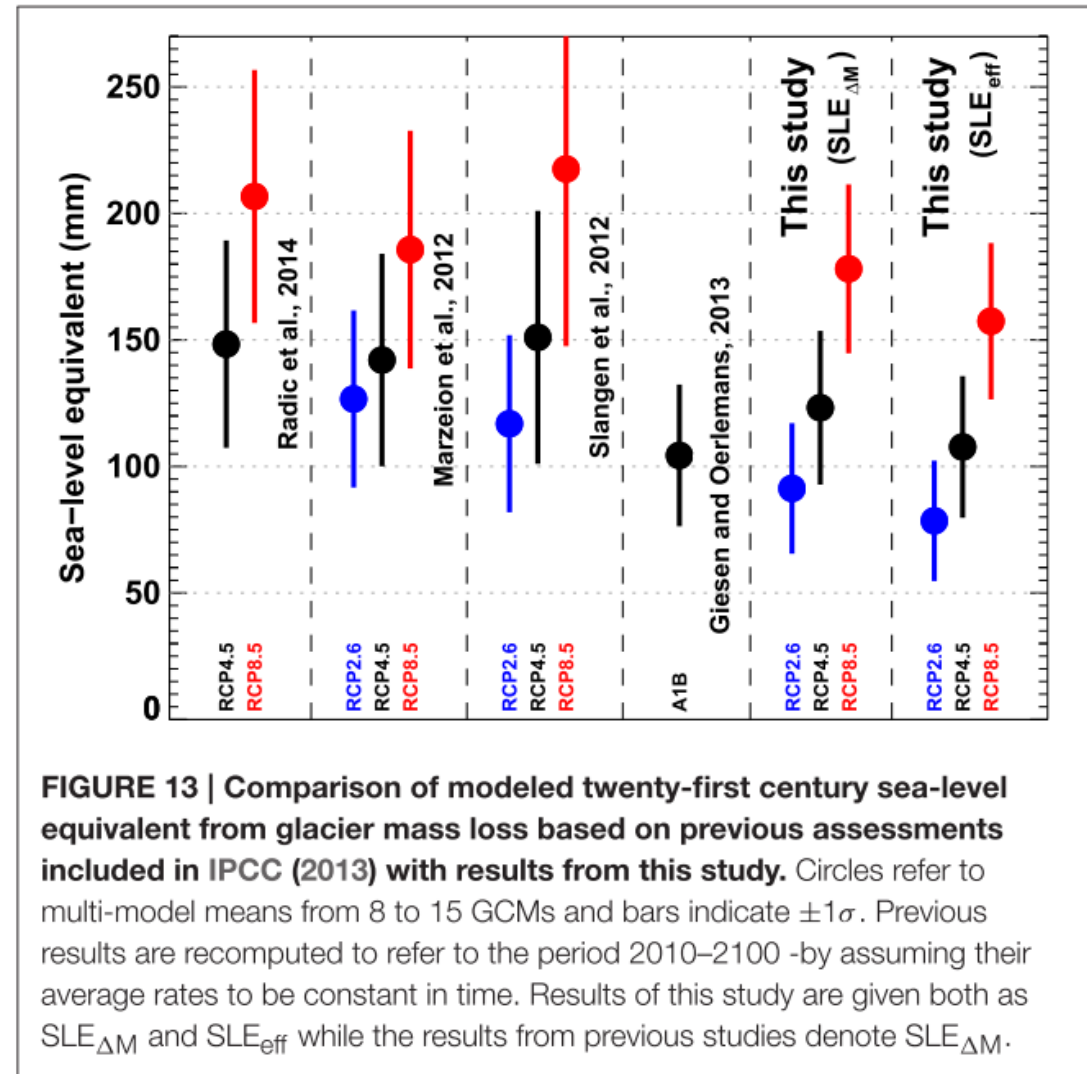


FIGURE 1 | Modeled retreat of (A) Great Aletschgletscher (land-terminating), Central Europe, and (C) Columbia Glacier (tide-water glacier), Alaska, according to the CanESM2 GCM and RCP4.5/RCP8.5. Calculated glacier surfaces are shown in 10-year intervals. Area-elevation distribution in 100 m bins is shown for today (gray) and 2100 (hatched). (B,D) Temporal evolution of mass balance components. Yearly values of annual and winter surface balance are shown as thin lines. Thick lines refer to 11-year running means. Note that refreezing is enlarged by a factor 10.

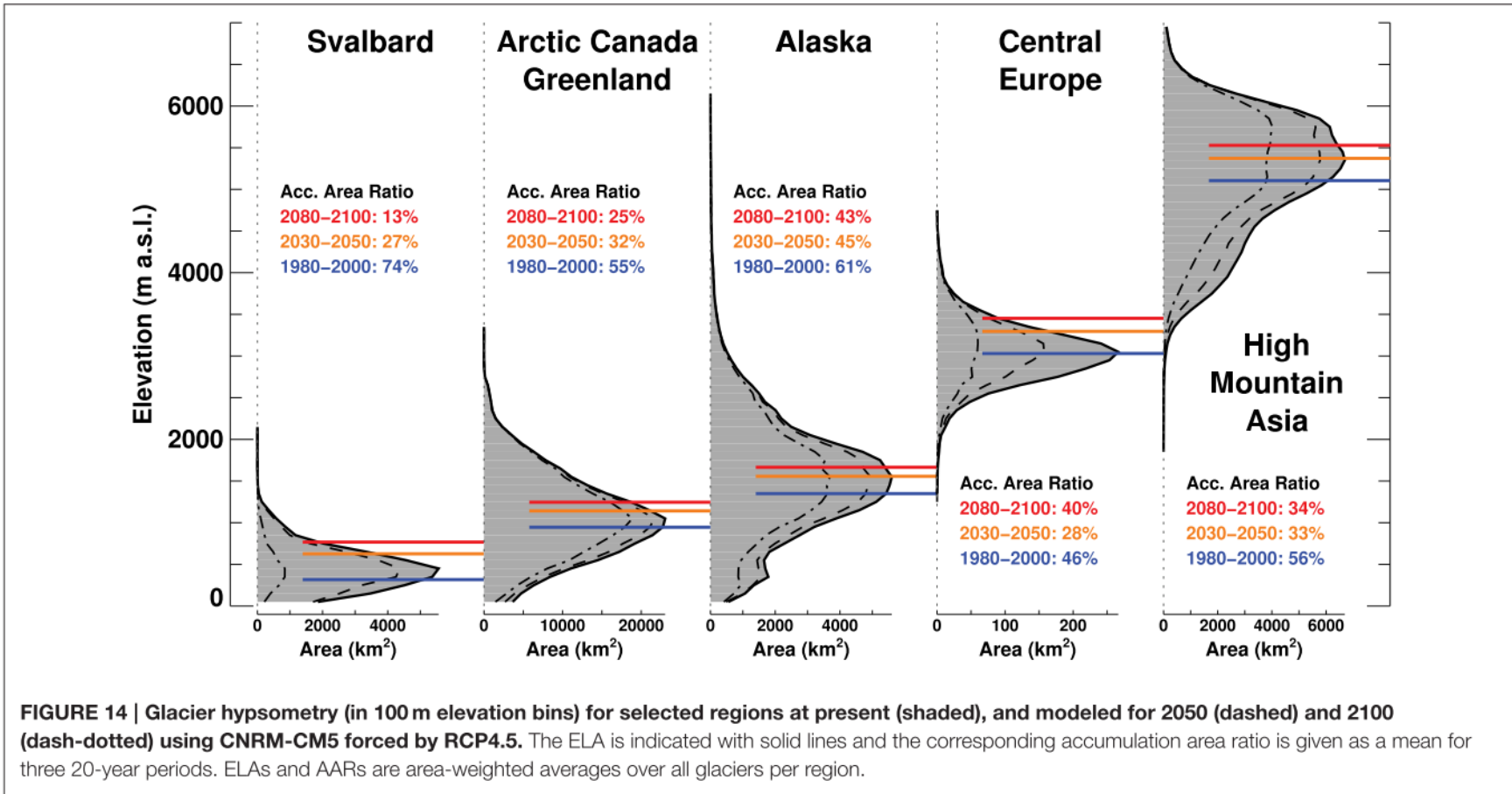
3 - Results



4a – Discussion – Results from other Models



4b – Discussion – Regional Differences





Practicals

- Energy Balance of a Debris Covered Glacier
 - Lapsing from off to on glacier
 - Discussing Fluxes
 - Converting fluxes to Melt
 - Sensitivities
- Mass Balance Model (?)

